Zoological Journal of the Linnean Society, 2024, XX, 1–28
https://doi.org/10.1093/zoolinnean/zlae005
Advance access publication 1 March 2024
Original Article

Original Article

Revision of the genus *Robbea* (Stilbonematinae: Desmodoridae), worldwide abundant marine nematodes with chromophoric Fe–Br inclusions and the description of a new stilbonematine genus

Florian Scharhauser[1], Daniel E.M. Saavedra[1], Philipp Pröts[1], Jörg A. Ott[1], Benedikt Geier[2,3], Harald R. Gruber-Vodicka[2,4], Maxim Polikarpov[5], Gleb Bourenkov[5] and Nikolaus Leisch[*,2,6]

[1]Department for Functional and Evolutionary Ecology, University of Vienna, Vienna, Austria
[2]Max Planck Institute for Marine Microbiology, Bremen, Germany
[3]Stanford University, School of Medicine, Department of Paediatrics and Infectious Diseases, CA, USA
[4]Zoological Institute, Christian-Albrechts-University, Kiel, Germany
[5]European Molecular Biology Laboratory, Hamburg unit c/o DESY, Hamburg, Germany
[6]European Molecular Biology Laboratory, Heidelberg, Germany

[*]Corresponding author. Max Planck Institute for Marine Microbiology, Celsiusstr. 1, 28205 Bremen, Germany. E-mail: nleisch@mpi-bremen.de

ABSTRACT

Nematodes are one of the most widespread and abundant animal taxa across aquatic and terrestrial environments. In marine shallow-water, porous sediments, members of the subfamily Stilbonematinae may be found in high numbers. Stilbonematinae are characterized by their coat of symbiotic bacteria, which give the nematodes a white appearance, while the nematodes themselves are usually colourless. We identified several species of the genus *Robbea* (Desmodoridae: Stilbonematinae) in which live specimens had a conspicuous dark purple coloration of the glandular sense organs (GSOs), highly specialized epidermal glands that are prominent in the Stilbonematinae. The dark inclusions in the GSOs of *Robbea* contained high concentrations of iron and bromide, regardless of their habitat. Morphological and phylogenetic analyses show that the genus *Robbea* is paraphyletic and we define the new genus *Cyathorobbea* gen. nov. for species with sucker-shaped post-pharyngeal supplements in males. Furthermore, we describe five new *Robbea* species from around the world. Some *Robbea* species are morphologically very similar and required the use of principal component analysis of morphometric data to untangle the diversity in this taxon. Our work emphasizes the value of live animal observations that enable the identification of important characters and highlights the overlooked diversity within the Stilbonematinae.

Keywords: µCT; EDX; morphometrics; molecular phylogeny; thiotrophic symbiosis

Abbreviations: ann, annulation; bac, bacteria; bbac, beginning of bacterial coat; b, bulbus; cc, cephalic capsule; cs, cephalic setae; c, corpus; cut, cuticle; cp, cuticular pore; fa, fovea amphidialis; fp, finger-like papillae; g, gut;gb, gubernaculum; hc, honeycomb structure; i, isthmus;in, inclusions; ls, labial sensillae; nr, nerve ring; scs, subcephalic setae; sp, spiculum; spt, spinneret; t, testis.

INTRODUCTION

Nematodes are one of the most abundant and widely distributed taxa on Earth. A significant part of this abundance and diversity is present in marine sediments where nematodes are important members of the meiofauna communities (Moens *et al.* 2013). In intertidal and subtidal shallow waters around the globe, a conspicuous subfamily within the Desmodoridae—the Stilbonematinae—can be found (Ott *et al.* 2004). They are characterized by an obligate ectosymbiosis with *Candidatus* Thiosymbion, a genus of chemoautotrophic sulphur-oxidizing Gammaproteobacteria (Polz *et al.* 1994, Zimmermann *et al.* 2016). The symbionts form a coat on the nematode's cuticle and give the otherwise colourless live specimens a bright-white appearance in incident light. The clades of symbionts are specific to host genera, and species-specific host–symbiont coupling occurs (Zimmermann *et al.* 2016). In addition to the phylogenetic

Received 9 June 2023; revised 22 December 2023; accepted 8 January 2024

specificity, the morphology of the symbiont cells and coats are specific to host genera and can be used as a character in host identification (Scharhauser *et al.* 2020).

The nematodes migrate through the chemocline in the sediments to provide their ectosymbionts with both oxygen and sulphide, and in turn live off their symbionts (J. Ott and Novak 1989, Ott *et al.* 1991). Another unique trait of all Stilbonematinae, linked to their symbiotic association, are the glandular sense organs (GSOs). These highly specialized epidermal organs are arranged in eight rows along the whole nematode body (Nebelsick *et al.* 1992, Bauer-Nebelsick *et al.* 1995). The neurosecretory cells in GSOs are linked to the external environment via hollow setae and secret compounds involved in host–symbiont recognition and the initiation and maintenance of the symbiotic relationship (Bulgheresi *et al.* 2006, 2011). Recent studies showed that within this nematode subfamily, the bacterial ectosymbionts show an astonishing diversity of cell division modes, which makes them a promising model system for bacterial cell division (Leisch *et al.* 2012, 2016, Pende *et al.* 2014, 2018, Weber *et al.* 2019, 2022).

Despite the fact that the Stilbonematinae as a subfamily are well supported based on morphological and molecular data (Kampfer *et al.* 1998, van Megen *et al.* 2009, Tchesunov 2013), there is a surprising morphological diversity between the genera in some key characteristics, such as the structure of the somatic and head cuticle (Urbancik and Bauer-Nebelsick *et al.* 1996a, Urbancik and Novotny *et al.* 1996b), the shape of the amphidial fovea, the structure and number of male accessory organs, and the construction of the pharynx. The pharynx has been a focus in early taxonomic work to distinguish between genera, as Cobb (1920) described a distinct muscular corpus for the pharynx for the genus *Catanema*, based on the type of *Catanema exile*. Likewise, on the grounds of a conspicuously muscular corpus, Gerlach (1956) erected the genus *Robbea* with the type species *Robbea caelestis* from Brazil. Later he added a second species, *Robbea tenax* from the Maldives (Gerlach 1963). Gerlach was aware of the profound differences between the two species; however, the peculiar pharynx anatomy shared by the two species seemed to justify their congeneric status (Gerlach 1963). Using the presence of a muscular corpus as the major criterion, several assignments to either *Catanema* or *Robbea* were made. Inglis (1967) described *Catanema cobbi*, which was later transferred to the genus *Laxus* (Ott *et al.* 1995). Hopper and Cefalu (1973) reported *Catanema porosum* from Florida and Vitiello (1973) reported *Robbea gallica* from the Mediterranean Sea. Subsequently, Platt and Zhang (1982) synonymized the genera *Catanema* and *Robbea*, placing *R. caelestis* (Gerlach 1956), *R. tenax* (Gerlach 1963), and *R. gallica* (Vitiello 1973) into the genus *Catanema*. Tchesunov (2013) redefined the genus *Catanema*, including only species in which the amphidial fovea is reduced to a porus, and transferred all species with spiral amphids and muscular corpus (*C. porosum* Hopper and Cefalu 1973, *C. smo*, and *C. macintyrei* Platt and Zhang 1982) to the genus *Robbea*. Using molecular and morphological analyses, Armenteros *et al.* (2014a) described specimens from Cuba, that the authors identified as *Robbea porosum* (Hopper and Cefalu 1973). In parallel, three new species, *Robbea hypermnestra*, *R. ruetzleri*, and *R. agricola*, were described by Ott *et al.* (2014) from Belize that have several conflicting morphological diagnoses and mismatches in their molecular data compared to *Robbea porosum sensu* Armenteros (2014b).

In this study, we resolve this decades-old taxonomic riddle by amending the description of *Robbea* (Gerlach 1956) based on our descriptions of one new species from the Caribbean Sea, two species from the Mediterranean, and two species from the West Pacific. All these species comply with the initial genus description *sensu* Gerlach (1956), but in contrast to all known Stilbonematinae (many of which have not been observed live), live specimens have noticeable dark inclusions in their GSOs, giving the nematode a conspicuously dark, dotted appearance. Based on 18S rRNA and *COI* marker gene analyses, and statistical morphometrics, we assign the five novel species to the genus *Robbea*. Additionally, we erect the new genus *Cyathorobbea* for those species that have colourless GSOs and share the key trait with *R. tenax* Gerlach (1963) that males have sucker-like postpharyngeal supplements, which is supported by molecular data.

MATERIALS AND METHODS

Nematode sampling, photo-vouchering, and fixation

Sediment samples were taken with cores or buckets with either skin or scuba diving (see Supporting Information, Table S1 for samples and sampling locations). Meiofauna was extracted with the stirring and decantation method using a 63-µm mesh sieve. Organisms were transferred to Petri dishes, single nematode specimens were handpicked under a dissection microscope, washed in 0.2 µm-filtered seawater, relaxed in $MgCl_2$, and identified under a compound microscope.

Specimens were fixed for morphology in 1X PBS-buffered 4% formaldehyde or in 3.5% glutaraldehyde, and for molecular work in 70% or 100% ethanol or RNAlater. Specimens for molecular analyses where all photo-vouchered (Supporting Information, Table S1). Slides with holotype and paratypes were deposited in the Natural History Museum Vienna, deposition numbers can be found in the Supporting Information, with each species description.

Microscopy

Specimens were transferred to a mixture of glycerine and water (ratio 1 : 9), the water was slowly evaporated, and the specimens mounted in pure glycerine. Light micrographs for vouchering were taken with an EOS 400 camera (Canon, Japan) mounted either on a Zeiss microscope (Zeiss Standard 14) (Zeiss, Germany) or on a Zeiss Jenamed 2 microscope (Zeiss, Germany). Detailed light micrographs were taken with a Zeiss Axio Imager A1 (Zeiss, Germany) and camera lucida drawings were produced using a Diavar microscope (Reichert, Austria). One adult male specimen from Carrie Bow Cay (CBC), Belize was observed with a Leica SP5 II confocal laser scanning microscope (CLSM) (Leica Microsystems, Germany). Confocal image stacks of auto fluorescent signals were acquired with the LAS AF Software (Leica) and volume renderings were computed with the volume rendering module of Amira 6.4 (Thermo Fisher Scientific, USA). The image processing software FIJI (Schindelin *et al.*, 2012) was used to extract a suitable longitudinal optical section of the pharynx.

Electron microscopy

For scanning electron microscopy (SEM) an adult female specimen from Carrie Bow Cay, Belize, was fixed in 2.5%

glutaraldehyde and post-fixed with 1% osmium tetroxide, dehydrated in a stepwise ethanol series (20–100% in 10% steps), critical point dried with a Leica EM CPD300 (Leica Microsystems, Germany), and sputter-coated with gold using a JEOL JFC-2300HR (JEOL Ltd, Japan). Images were acquired with a Philips XL 30 ESEM (Philips, Netherlands), and brightness and contrast were adjusted in Adobe Photoshop CS2 or FIJI. For energy-dispersive X-ray spectroscopy (EDX) analyses, the live specimens were transferred to distilled water and then dried on a SEM stub. Elemental analyses were performed on eight *Robbea* and eight *Catanema* specimens (see Supporting Information, Table S1) with a JEOL microscope with an EDX Element Analysis System at an accelerating voltage of 25 kV. The specimen used for micro-computed tomography (µCT) was serially sectioned at 1.5-µm section thicknesses using a Leica UC7 ultramicrotome. Sections of interest were transferred to a SEM stub, carbon coated using a Leica ACE600, and imaged with a backscatter detector in a FEI FEG SEM.

Micro-computed tomography analyses

For µCT analyses, a specimen from Carrie Bow Cay, Belize, was fixed in 2.5% glutaraldehyde buffered in 3X PHEM pH 7.4 (Montanaro *et al.*, 2016) and post-fixed in 1% osmium tetroxide. The sample was dehydrated via a stepwise ethanol series then transferred into pure acetone, and infiltrated and embedded in agar low-viscosity resin using centrifugation embedding, according to McDonald (2014). The sample was trimmed and mounted onto a SPINE sample holder (Cipriani *et al.* 2006). Measurements were carried out on the EMBL undulator beamline P14 at the PETRA-III storage ring (c/o DESY, Hamburg, Germany) using the propagation-based phase-contrast imaging setup described in Polikarpov *et al.* (2019) For details on X-ray imaging and data processing, see methods in Supporting Information.

Statistical analyses of morphological characters and species delimitation

We recorded 25 metrics of 41 *Robbea* specimens (Supporting Information, Table S2) and corresponding measurements of *Catanema porosum*, *C. macintyrei*, *C. smo*, *Robbea caelestis*, *R. porosum*, *R. gallica*, *R. gerlachi*, *R. tenax*, *R. hypermnestra*, *R.ruetzleri*, *R. agricola*, and *Robbea* sp. (*sensu* Tchesunov 2013) were retrieved from the literature. All statistical analyses were performed with R software R v.4.2.2 (R Team 2009).Variables were tested for homogeneity of variances using the Bartlett test (Stevenson and Howard 1937). Sex-specific morphological characteristics were excluded from further analysis. A one-way analysis of variance (one-way ANOVA) (Whitley and Ball 2002) with post-hoc test (Tukey's HSD) (Tukey 1949) and a *t*-test with Bonferroni correction (Bonferroni 1936) were conducted for each variable. The 14 variables with significant variances between clusters were used for a principal component analysis (PCA) with the 'factoextra' package in R (Kassambara and Mundt 2020). The same data were used for a cluster analysis using the 'pvclust' package (Suzuki *et al.* 2019) with the unweighted pair-group method using arithmetic averages (UPGMA) clustering method with squared Euclidian distance as a measure of dissimilarity and a multiscale bootstrap resampling of 1000.

DNA extraction, amplification, and genetic barcoding

The DNA of 21 *Robbea* and one *Catanema* specimens (Supporting Information, Table S1) was extracted with the DNeasy Blood and Tissue Kit (Qiagen, Hilden, Germany) following the manufacturer's instructions with two modifications: digestion with proteinase K was extended to 14 h and the elution step was done with 100 µL of elution buffer. For DNA barcoding, a partial 18S rRNA gene fragment (≥1000 bp) of the nematode was amplified with the nematode specific primers 466f (CCACATCCAAGGAAGGCAG) and 1548r (ATTCCTTCAGTGTAGCGCG) (Ott *et al.* 2020) with the following cycling conditions: 5 min at 95°C followed by 35 cycles of 30 s at 95°C, 45 s at 60.7°C, and 1.2 min at 72°C, final extension step of 10 min at 72°C. For symbiont 16S RNA amplification general primers 27f (5′-AGAGTTTGATCMTGGCTCAG-3′) (Weisburg *et al.* 1991) and 1492R (5′-GGY TAC CTT GTT ACG ACT T-3′) (Loy *et al.* 2005) were used with the following conditions: 3 min at 95°C followed by 35 cycles of 30 s at 95°C, 30 s at 55°C, and 1.5 min at 72°C, final extension step of 10 min at 72°C.

Quality and length of the PCR products were checked with gel electrophoresis, purified with ExoSAP-IT™ PCR Product Clean-up (Applied Biosystems, USA) and sequenced at MicroSynth (MicroSynth, Switzerland).

Metagenome sequencing

Ten specimens (Supporting Information, Table S1) were prepared for low-coverage metagenome sequencing at the Max Planck Centre for Plant Genetics, Cologne. Library preparation was performed with the Ovation Ultralow Library Systems kit (NuGEN Technologies, US) with 1–5 ng DNA input per specimen. Illumina library size selection was done with an agarose gel. Either 2 × 100 bp or 2 × 150 bp paired-end reads were sequenced on an Illumina HiSeq 3000 (Illumina, USA) for each individual (8–25 million reads each).

Bioinformatics and phylogenetic analyses

Adapters and low-quality bases (Q > 2) were trimmed with bbduk (Bushnell 2014) and reads longer than 36 bp were used for metagenome assembly with (Meta)SPAdes 3.1–3.9 (Bankevich *et al.* 2012). The full-length mitochondrial *COI* gene of nine *Robbea* specimens were extracted with BANDAGE (Wick *et al.* 2015) using the built-in BLAST database option and closely related *COI* from stilbonematine nematodes. PhyloFlash was used to reconstruct the ribosomal small subunit 18S rRNA gene sequence of the host and the ribosomal small-subunit 16S rRNA gene (16S) of the ectosymbionts (Gruber-Vodicka Harald R. *et al.* 2020).

We retrieved 270 nematode 18S rRNA sequences with a minimum length of 1300 bp from previous publications (Ahmed and Holovachov 2020, Ahmed *et al.* 2020, Pereira *et al.* 2020, Scharhauser *et al.* 2020) and added 10 new *Robbea* and one new *Catanema* sp. (see Supporting Information, Table S1: *Catanema* sp. '*thin*') 18S full-length sequences.

For an extended 18S analysis, we combined previously published sequences (see above) with a minimum length of 700 bp with new PCR-based 18S rRNA sequences of one ***Robbea weberae* sp. nov.** (this publication) and eight ***Robbea lotti* sp.**

nov. (this publication) specimens resulting in a dataset of 492 sequences.

For the nematode full-length *COI* analysis, we combined nine *Robbea* and one *Catanema* sp. '*thin*' sequences with the dataset of Scharhauser *et al.* (2020), and 44 published nematode sequences as an outgroup. We created a second *COI* gene matrix with a total of 94 *COI* gene sequences where we included partial *COI* sequences (min. 393 bp) as in Scharhauser *et al.* (2020) to compare to the already published stilbonematine sequences in Armenteros *et al.* (2014b). All *COI* gene sequences were translated into amino acid sequence before alignment.

For the bacterial phylogeny, the 16S rRNA sequences of the ectosymbionts of nine *Robbea* specimens from five species, two *Catanema schiemeri* and one *Catanema* sp. '*thin*' specimens were combined with the dataset of (Scharhauser *et al.* 2020) resulting in 93 sequences.

All sequences were aligned using MAFFT v.7 (Katoh and Standley 2013) using the Q-insi option (Katoh and Toh 2008) for the 16S and 18S and the E-insi option for the *COI* dataset. The optimal substitution model for each alignment was chosen by ModelFinder (Kalyaanamoorthy *et al.* 2017) and are TIM3e+I+G4 for the 18S alignment, mtZOA+F+G4 model for the *COI* alignment, and TIM+F+I+G4 for the 16S alignment. All alignments are deposited at figshare: 10.6084/m9.figshare.23303633.

All phylogenetic analyses were performed with the maximum-likelihood based software IQTREE v.1.6.12 (Nguyen *et al.* 2015) with the Ultrafast Bootstrap Approximation UFBoot option using 10 000 iterations (Minh *et al.* 2013). Additional support values were generated by using approximate Bayes (aBayes) (Anisimova *et al.* 2011) and SH-aLRT analyses (Guindon *et al.* 2010). Raw trees were plotted with FigTree (https://github.com/rambaut/figtree) and arranged with Adobe Illustrator (Adobe Inc., USA).

RESULTS

Discovery of new *Robbea* species

We collected specimens of nine *Robbea*-like species from 10 different locations in the Caribbean Sea, the Mediterranean Sea, the Red Sea, and the Pacific (Fig. 1C). All collected live specimens showed a conspicuous dark coloration caused by inclusions within their GSOs, independent of their sampling site (Fig. 2). All these dark-coloured specimens conformed to the genus definition of the type species, *Robbea caelestis* Gerlach 1956. For species that had been previously described as either *Robbea* or *Catanema*, we distinguished all species *sensu Robbea* Gerlach 1956 from species with the characteristics of *Robbea tenax* Gerlach 1963. For the latter species we propose the new genus, ***Cyathorobbea* gen. nov.**. An emended diagnosis of *Robbea* Gerlach 1956 and a formal definition of the new genus are given below. In short, the genera *Robbea* and *Cyathorobbea* show clear differences in: (i) the coloration of live specimens, caused by the coloration of the GSOs; (ii) the size; (iii) the length/with ratio; (iv) the head and somatic setation; (v) the different shapes of the amphidial fovea; and (vi) the absence of male supplements in *Robbea* (for details see Table 1). The presence of conspicuous dark inclusions in the GSOs, observed in all the newly described *Robbea* species, is potentially a key character for the genus. This cannot be verified for species described previously, due to the lack of live observations, and the fact that the specimens lose the coloration upon fixation with aldehyde- and alcohol-based fixatives.

The genus *Robbea* Gerlach 1956

Diagnosis Stilbonematinae

Desmodoridae, with short, unarmed pharynx; minute buccal cavity; pharynx three partite, corpus may be distinctly muscular and swollen, thin isthmus containing nuclei, bulbus round, muscular or mainly glandular; cuticle finely transversely striated or coarsely annulated; amphidial fovea spiral, loop shaped or reduced to a porus; cuticle covered by ectosymbiotic sulphur-oxidizing chemoautotrophic gamma proteobacteria.

Emended diagnosis of the genus Robbea

Stilbonematinae; body long (L = 2.8–8.3 mm), slender (a > 110), cuticle thin, transverse striation extremely fine, cephalic capsule with block layer, creating a honey-comb structure in surface view; first circle of cephalic sensillae as six finger-like papillae retracted into mouth opening, second circle as six conical papillae (<1 μm long) at margin of buccal membrane in lateral and submedian positions; four long cephalic setae in sublateral position, directed anteriorly, close to the anterior margin of the amphidial fovea; one circle of eight subcephalic setae with four in submedian position (either at about the level of the cephalic setae or at the level of the centre of the amphidial fovea) and four sublateral near the posterior margin of the amphidial fovea. Somatic setae minute or absent, except for subventral rows of papilliform setae on the male tail, instead eight rows of cuticular pores corresponding to the GSOs; GSOs in eight rows, two sublateral rows on each side and two submedian rows dorsally and ventrally, respectively. GSOs dark-purple coloured in live animals only. Amphidial fovea flat with shallow spiral groove, ventrally wound. Pharynx with distinctly swollen muscular corpus, distinctly set off from the long and thin isthmus, small mainly glandular terminal bulb. Spicules curved, cephalate, capitulum appearing heart-shaped under the light microscope, gubernaculum with paired dorsocaudally directed plate-shaped apophysis with reinforced margin; tail cylindro-conical. Vulva with conspicuous sclerotization.

Dense monolayer of ectosymbiotic coccobacilli attached to the cuticle, starting several pharynx-lengths from anterior end to near tip of tail. Body diameter decreases at onset of bacterial coat, accommodating the thickness of the symbiont layer. Bacteria arranged with their longer axis parallel to the nematode's cuticle, dividing transversally (see Figs 2 for an overview of host and symbiont characteristics).

Remarks: Whether the dark coloration of the GSOs can be used as a genus character is unclear. The lack of coloration in all species that had not been observed live is most probably due to the fixation and processing of the nematodes prior to observation, which leads to a fading of the colour. This underlines the importance of observation of live material in the study of meiofauna.

List of species

Robbea caelestis Gerlach 1956 (type species)
R. gallica Vitiello 1973

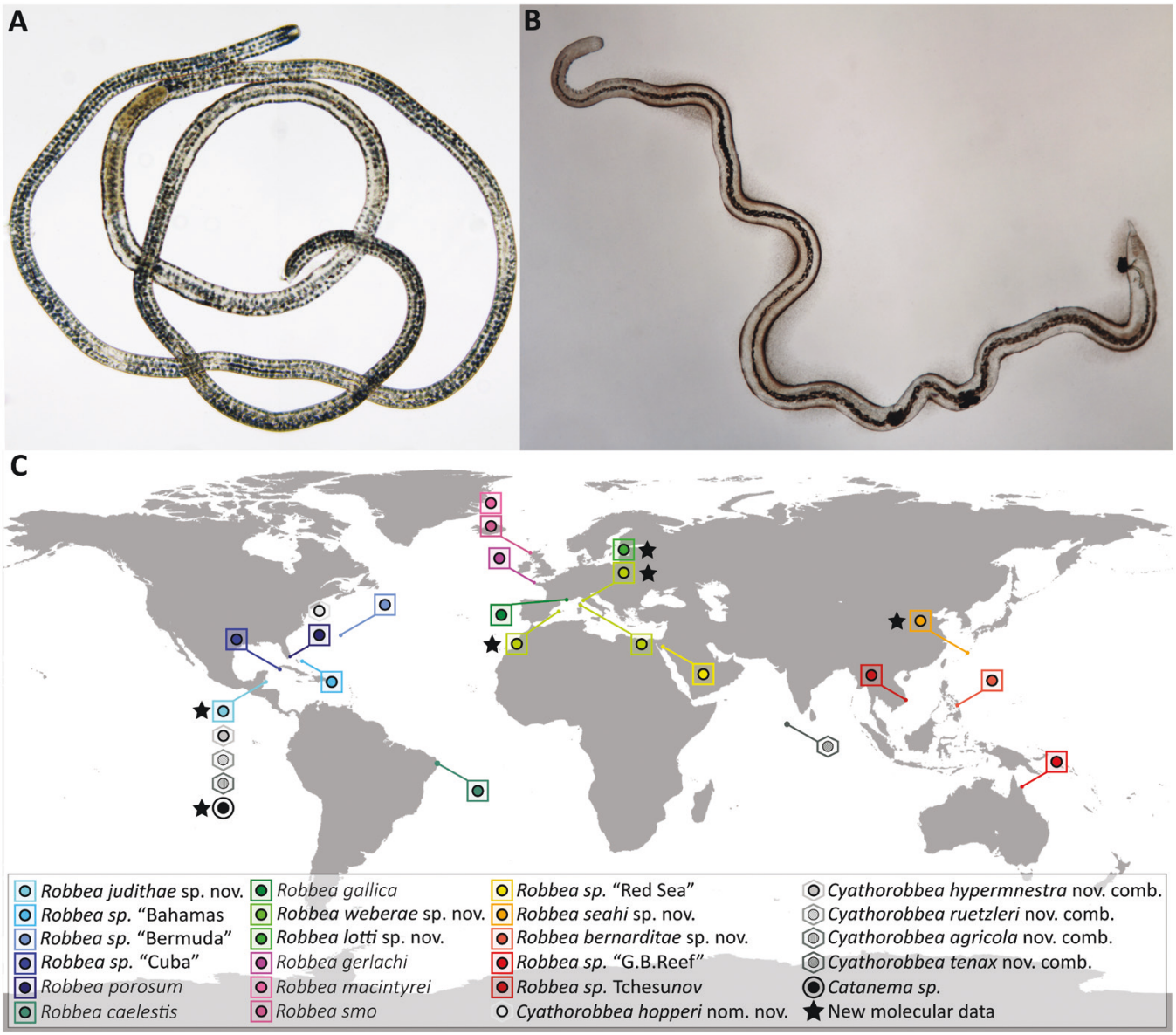

Figure 1. Live specimens and global occurrence of *Robbea* and *Cyathorobbea* species. A, *Robbea judithae* with typical dark GSOs. B, *Cyathorobbea hypermnestra* without dark GSOs and with symbionts in the gut. C, sampling sites of new and previously described *Robbea* and *Cyathorobbea* species.

R. porosum (Hopper and Cefalu 1973) Tchesunov 2013
Syn: *Catanema porosum* Hopper and Cefalu 1973

R. macintyrei (Platt and Zhang 1982) nov. comb.
Syn: *Catanema macintyrei* Platt and Zang 1982

R. smo (Platt and Zhang 1982) nov. comb.
Syn: *Catanema smo* Platt and Zang 1982

R. judithae sp. nov. this publication
R. weberae sp. nov. this publication
R. lotti sp. nov. this publication
R. seahi sp. nov. this publication
R. bernarditae sp. nov. this publication

The following specimens are tentatively assigned to the genus *Robbea*:

R. sp. Tchesunov 2013
R. sp. 'Bahamas', *R.* sp. 'Bermuda', *R.* sp. 'Red Sea', *R.* sp. 'Great Barrier Reef' (this publication)
R. sp. 'Cuba' [*R. porosum* in Armenteros *et al.* (2014b)]

TAXONOMY

Class Chromadorea Inglis 1983

Subclass Chromadoria Pearse 1942

Order Desmodorida De Coninck 1965

Suborder Desmodorina De Coninck 1965

Superfamily Desmodoroidea Filipjev 1922

Family Desmodoridae Filipjev 1922

Subfamily Stilbonematinae Chitwood 1936

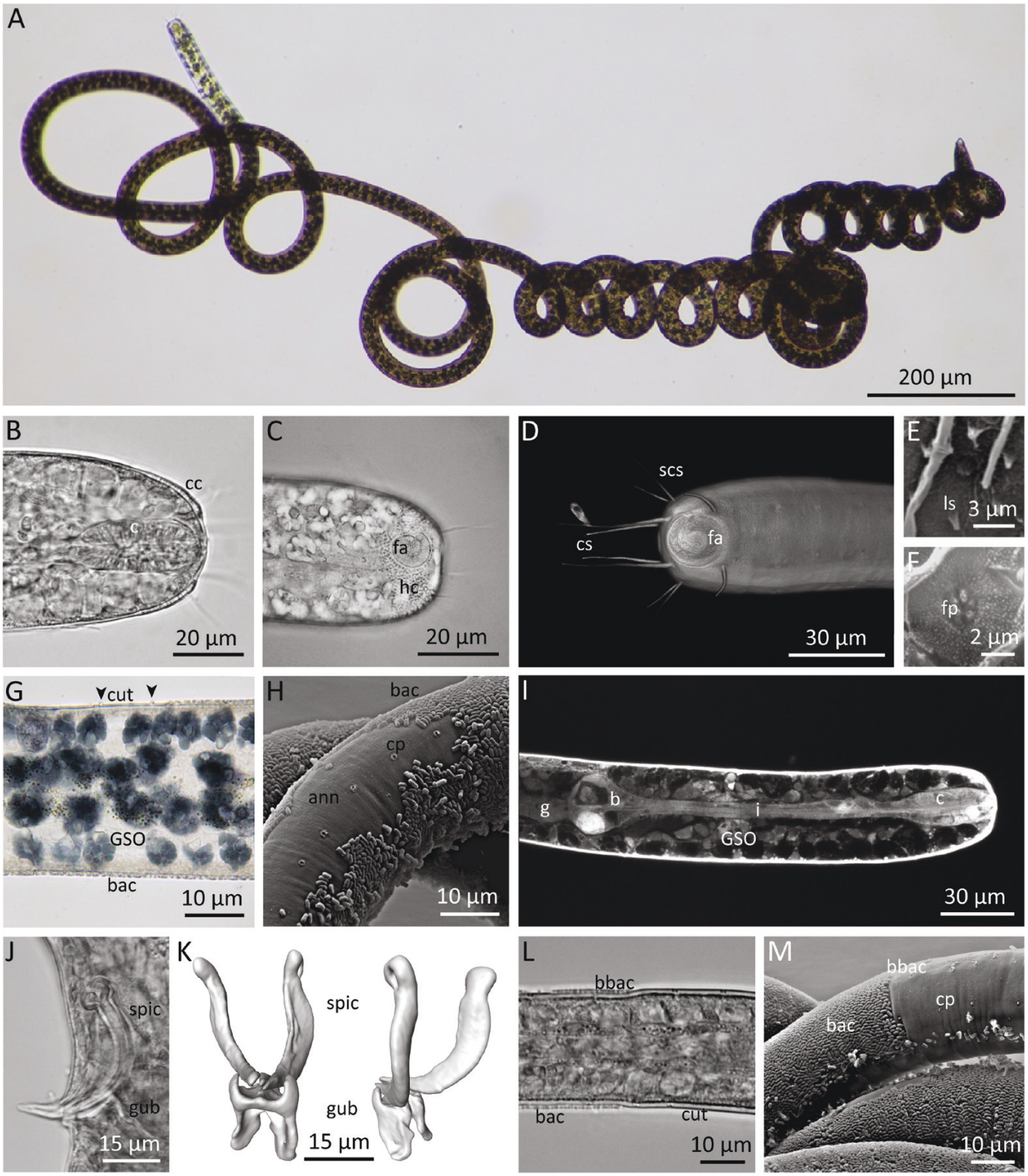

Figure 2. Characteristics of the genus *Robbea*. A, total view of a live *R. seahi* sp. nov.. The transparent anterior body part is symbiont free, the opaque appearance of the rest of the body is due to the symbiont coat. The rows of dark coloured GSOs extend throughout the body. LM B-M Morphological details of *R. judithae* sp. nov.. B, anterior end, optical section. LM of preserved specimen. C, anterior end, surface view. LM of live specimen D, volume rendering of a CLSM stack showing setation of anterior end. E, mouth opening surrounded by circle of six papilliform outer labial sensillae, SEM. F, inner labial sensillae in form of six finger-like papillae retracted into mouth opening, SEM. G, midbody, lateral view, optical section. Double row of lateral GSOs, in median rows the connection to the outside via pores is visible (arrowheads). LM of live specimen. H, SEM of midbody region showing rows of cuticular pores and annulation where the coat of symbiotic bacteria is disrupted. I, CLS micrograph of pharyngeal region showing muscular corpus, thin isthmus and small, glandular bulbus. J, spiculum of holotype, LM. K, spicula and gubernaculum, ventral and oblique dorsal views. µ-CT images. L, optical section showing edge of bacterial coat with reduction of bacterial coat. The reduction of body diameter from the symbiont-free anterior end (right) to the posterior body region (left), LM. M, SEM micrograph of same region.

Table 1. Morphological characteristics of the genera *Robbea* Gerlach 1956 and *Cyathorobbea* gen. nov.

	Robbea	*Cyathorobbea*
body length	2.8–8.3 mm	1.8–4.5 mm
a	110–257	40–101
head setation	4 cephalic setae 1 circle of 8 subcephalic setae	4 cephalic setae 2–3 circles of 8 subcephalic setae
somatic setation	absent or short setae, rows of pores	short and/or long setae throughout body
cup-shaped supplements in males	absent	present, in post-pharyngeal region
Glandular sense organs—GSOs	present, with dark inclusions, in some species enlarged and protruding GSOs in males	present, transparent, without dark inclusions
symbiont shape and arrangement	monolayer, small coccobacilli, dividing transversally	monolayer, diverse morphotypes, small coccobacilli or upright standing rods, rods dividing longitudinally

Genus *Robbea* Gerlach 1956

Robbea judithae sp. nov.

ZooBank registration: http://zoobank.org:urn:lsid:zoobank.org:act: EB683064-846B-4747-8431-E10DD10EFC2.

Type location: Carrie Bow Cay, Belize; back-reef sand patch north of the island, 2 m depth. Coordinates: 16.803371 N, 88.082003 W.

Type material: One holotype (NHMW-ZOO-EV-M-5863), four paratypes male (NHMW-ZOO-EV-M-5864/1-4), three paratypes female (NHMW-ZOO-EV-M-5865/1-3). Collection date: April 2013. Collector: J.A. Ott.

Other material: Several specimens in J.A. Ott collection.

Distribution: Regularly in all shallow, subtidal, back-reef sands around Carrie Bow Cay.

Etymology: The species is dedicated to Judith Zimmermann, who contributed significantly to the study of Stilbonematinae.

Description: With the characters of the genus. Measurements see Supporting Information, Table S2.

Large, slender species (Figures 3–5), live specimens with conspicuously dark-coloured GSOs. Males with prominent ventral GSOs in post-pharyngeal region that protrude as 16–18 bumps when the worm's body is bent ventrally. Cephalic capsule extending over 55–60% of corpus. Corpus of the pharynx less than 25% of pharynx length, isthmus very long occupying 61–67% of pharynx, bulbus small, glandular. Tail conical with rounded tip. Symbiotic bacteria short rods, 2 × 1μm.

Robbea weberae sp. nov.

ZooBank registration: http://zoobank.org: urn:lsid:zoobank.org:act:00CF1524-8B96-40F2-8A40-EC4AEC20BD99.

Type location: Bay of Sant' Andrea, Elba, Italy; subtidal sand in 5–6 m depth. Coordinates: 42.808342 N, 10.141764 E.

Type material: One holotype (NHMW-ZOO-EV-M-5866), five paratypes male (NHMW-ZOO-EV-M-5867/1-5), two paratypes female (NHMW-ZOO-EV-M-5868/1-2). Collection date: April 2016. Collector: F. Scharhauser.

Other material: Several specimens in J.A. Ott collection.

Etymology: The species is dedicated to Miriam Weber, scientist and our host at the Hydra Marine Station, Elba.

Description: With the characters of the genus. Measurements see Supporting Information, Table S2.

Large (L > 7mm), extremely slender (a > 200) species, females with much shorter tail than males (Figures 6 and 7). Post-pharyngeal ventral GSO enlarged but not protruding. Cephalic capsule extending over 55–60% of corpus. Corpus about 25% of pharynx length, isthmus 60–63%, bulbus 13–17%. Cuticle extremely finely striated, striae 0.4 μm wide. Vulva strongly cuticularized. Tail conical with rounded tip. Symbiotic bacteria rods, 2.3–2.6X1 μm.

Robbea lotti sp. nov.

ZooBank registration: http://zoobank.org: urn:lsid:zoobank.org:act:35EFD783-FDBC-4C54-B9B7-DDE69CABA765.

Type location: Bay of Sant' Andrea, Elba, Italy; subtidal sand in 5–6 m depth. Coordinates: 42.808342 N, 10.141764 E.

Type material: One holotype (NHMW-ZOO-EV-M-5869), three paratypes female (NHMW-ZOO-EV-M-5870/1-3). Collection date: April 2016. Collector: F. Scharhauser.

Etymology: The species is dedicated to Christian Lott, scientist and underwater film-maker at the Hydra Marine Station, Elba.

Description: With the characters of the genus. Measurements see Supporting Information, Table S2.

Shorter (L < 7mm) and stouter than the foregoing species (Figures 8 and 9). Cephalic capsule long, extending over >60% of corpus. Corpus about 25% of pharynx length, isthmus short with 47–54%, bulbus large, round, occupying one-fifth of the pharynx. Cuticle finely striated, striae 0.6μm wide. Vulva distinctly cuticularized, but less so than in the forgoing species. Tail conical with a distinctly 'pipette'-shaped tip. Symbiotic bacteria rods, 3 × 1.5 μm.

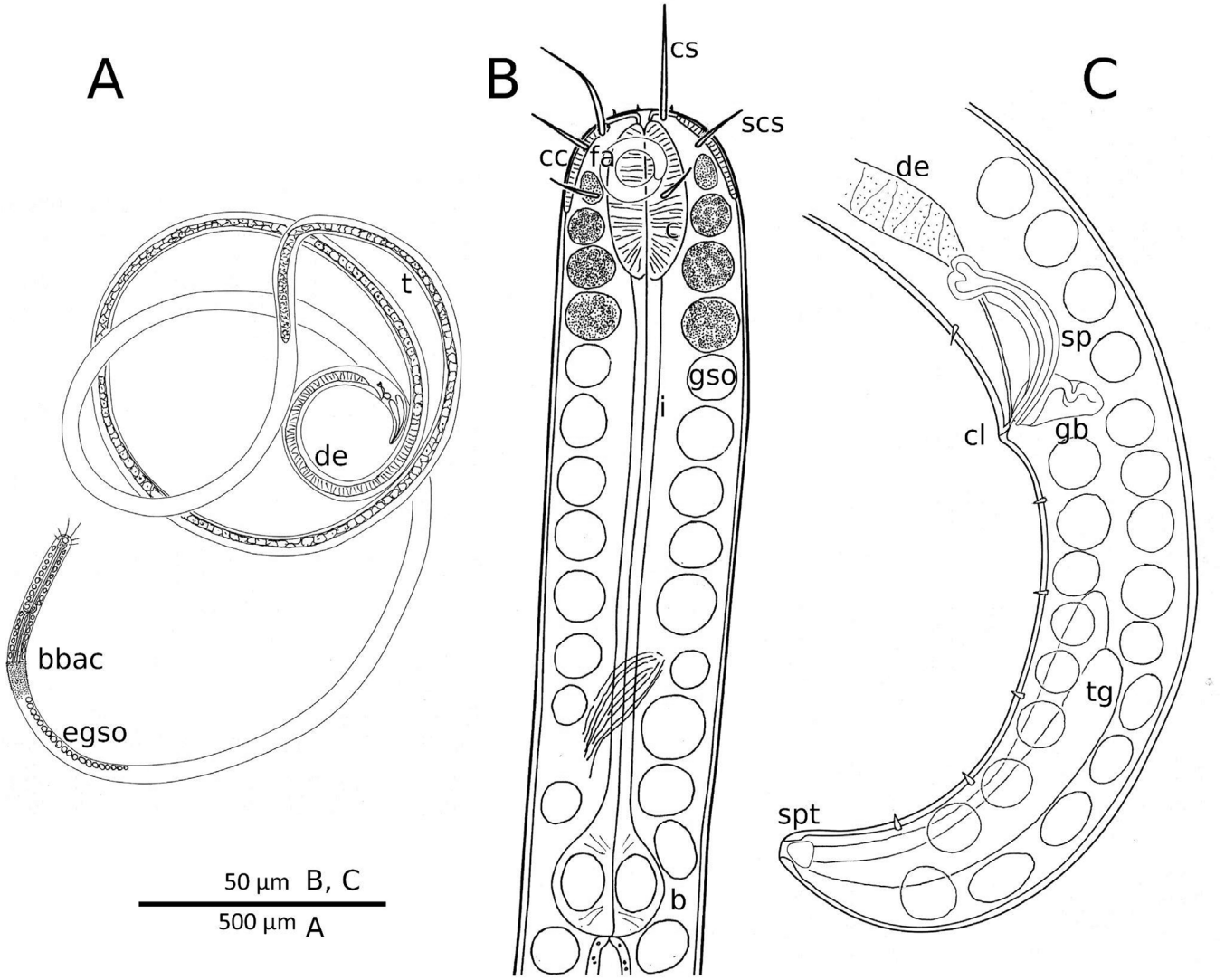

Figure 3. *Robbea judithae* sp. nov. male. A, total view of paratype. B, pharynx region of holotype. C, tail region of holotype. Abbreviations: bulbus, b; begin bacterial coat, bbac; corpus, c; cephalic capsule, cc; cloaca, cl; cephalic seta, cs; ductus ejaculatorius, de; enlarged glandular sense organs, egso; fovea amphidialis, fa; gut, g; gubernaculum, gb; isthmus, i; subcephalic seta, scs; spiculum, sp; spinneret, spt; testis, t; tail gland, tg.

Robbea seahi sp. nov.

ZooBank registration: http://zoobank.org: urn:lsid:zoobank.org:act:5B3D9322-A4D5-44FB-8B55-B45FC258C271.

Type location: Yakata, Okinawa, Japan; shallow subtidal sand. Coordinates: 26.4926 N, 127.842126 E.

Type material: One holotype (NHMW-ZOO-EV-M-5871), three paratypes male (NHMW-ZOO-EV-M-5872/1-3). Collection date: Dec. 2017. Collector: B. Seah.

Other material: Several specimens in J.A. Ott collection.

Etymology: The species is dedicated to Brandon Seah, marine scientist who collected the worms.

Description: With the characters of the genus. Measurements see Supporting Information, Table S2.

Small (<6 mm long) and slender species (Figures 10 and 11). Males with prominent, enlarged GSO in ventral post-pharyngeal region, protruding as 17–20 bumps. Subcephalic setae almost as long as cephalic setae. Cephalic capsule short, extending over about 50% of corpus. Corpus occupying about 25% of pharynx length, isthmus long (>60%), very small, round, glandular bulbus. Small somatic setae distributed over body. Tail conical with pointed tip. Symbiotic bacteria slender rods, 3,7 × 1.5 µm.

Robbea bernarditae sp. nov.

ZooBank registration: http://zoobank.org: urn:lsid:zoobank.org:act:3585C810-E79D-4E8C-A534-B6FE6AB23F14.

Type location: Punta, BayBay, Leyte, Philippines; intertidal, fine sand next to mangrove stand. Coordinates: 10.642584 N, 124.774708 E.

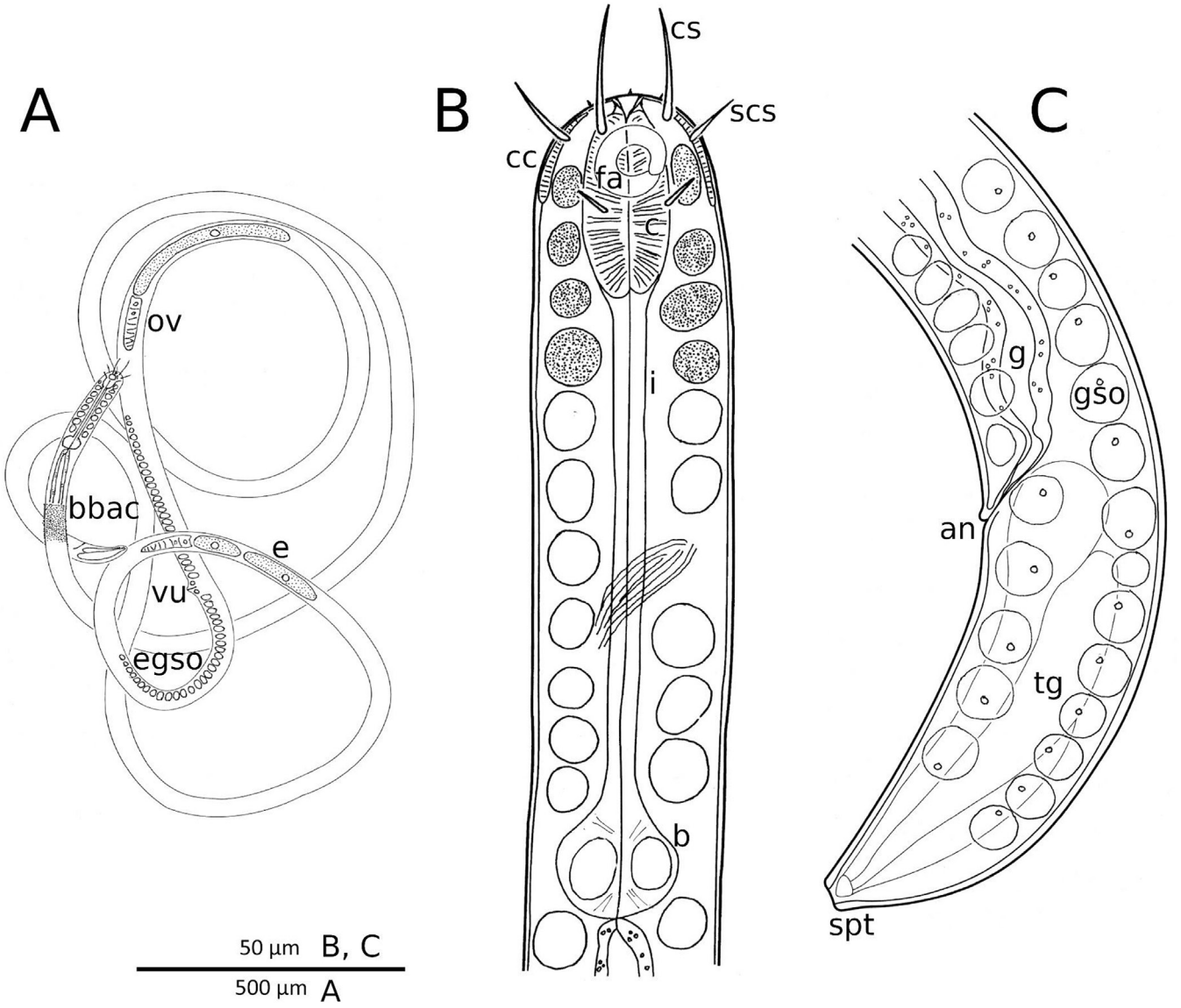

Figure 4. *Robbea judithae* sp. nov. female. A, total view of paratype. B, pharynx region of paratype. C, tail of paratype. Abbreviations: anus, an; bulbus, b; begin bacterial coat, bbac; corpus, c; cephalic capsule, cc; cephalic seta, cs; egg, e; enlarged glandular sense organs, egso; fovea amphidialis, fa; gut, g; gubernaculum, gb; glandular sensory organ, gso; isthmus, i; ovary, ov; subcephalic seta, scs; spiculum, sp; spinneret, spt; tail gland, tg; vulva, vu.

Type material: One holotype (NHMW-ZOO-EV-M-5873), one paratype male (NHMW-ZOO-EV-M-5874). Collection date: June 1996. Collector: J.A. Ott.

Etymology: The species is dedicated to Bernardita Germano-Pilapil, former student of J.A. Ott, native of Leyte, Philippines, who helped with collection of specimens.

Description: With the characters of the genus. Measurements see Supporting Information, Table S2 (excel sheet).

Very small (<<6 mm long) and rather stout species (Figures 12 and 13). Amphids more distinctly spiral than in other species. Males with prominent enlarged GSO in ventral post-pharyngeal region, protruding as 19 bumps. The species is remarkable for small (2 µm long) setae situated close to the submedian subcephalic setae. Cephalic capsule very long, extending over >70% of corpus. Long corpus occupies up to a third of pharynx length, large bulbus and consequently a very short isthmus (48–55% of pharynx length). Sparse somatic setae. Tail conical with rounded tip. Male testis with conspicuous large, round cells (sperm?). Symbiotic bacteria coccobacilli, 1.3 × 1 µm.

Robbea sp. Bahamas

Sampling location: Little Darby Island; 0.5 m, medium sand close to *Thalassia* bed. Coordinates: 23.857222 N, 76.216944 W.

Material: One female specimen in the collection of J.A. Ott.

Description: With the characters of the genus, measurements see Supporting Information, Table S2.

Very long (L > 8 mm) and slender (a > 200), cephalic capsule long (70% of corpus length), subcephalic setae 60% of cephalic setae, corpus 25% of pharynx length (Figure 14).

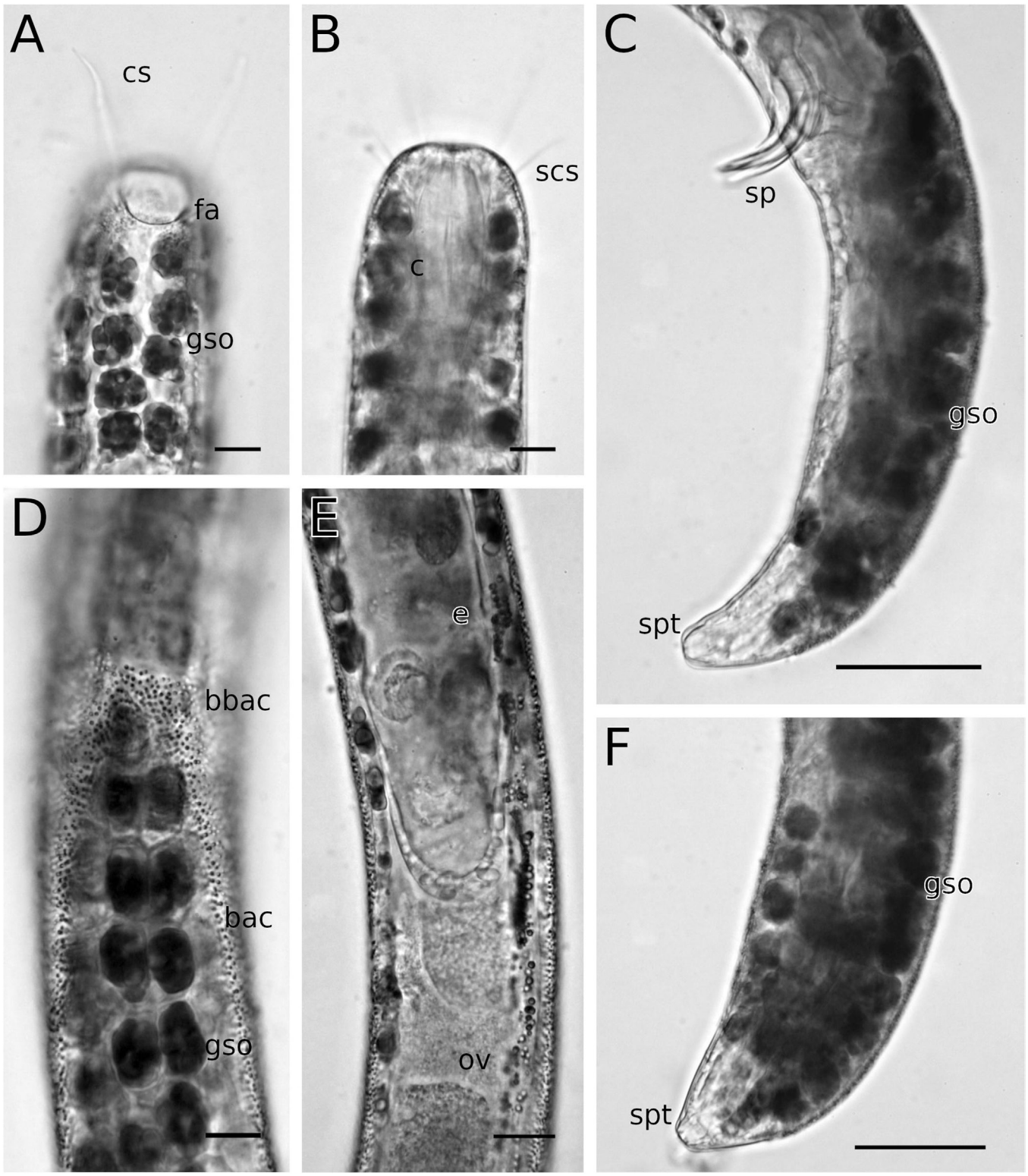

Figure 5. *Robbea judithae* sp. nov.. A, anterior end, surface view. B, anterior end, optical section. C, tail region of male. D, beginning of bacterial coat. E, anterior female gonad and egg. F, tail of female. LM of live specimens. Abbreviations: symbiotic bacteria, bac; beginning of bacterial coat, bbac; corpus, c; cloaca, cl; cephalic seta, cs; ductus ejaculatorius, de; egg, e; fovea amphidialis, fa; ovary, ov; subcephalic seta, scs; spiculum, sp; spinneret, spt. Scale bars: A, B, D, E, 10 μm; C, 20 μm; F, 5 μm.

Robbea sp. Bermuda

Sampling location: Nonsuch Island; 1 m, medium sand close to *Thalassia* bed. Coordinates: 32.348079 N, 64.664433 W.

Material: One female specimen in the collection of J.A. Ott.

Description: With the characters of the genus, measurements see Supporting Information, Table S2.

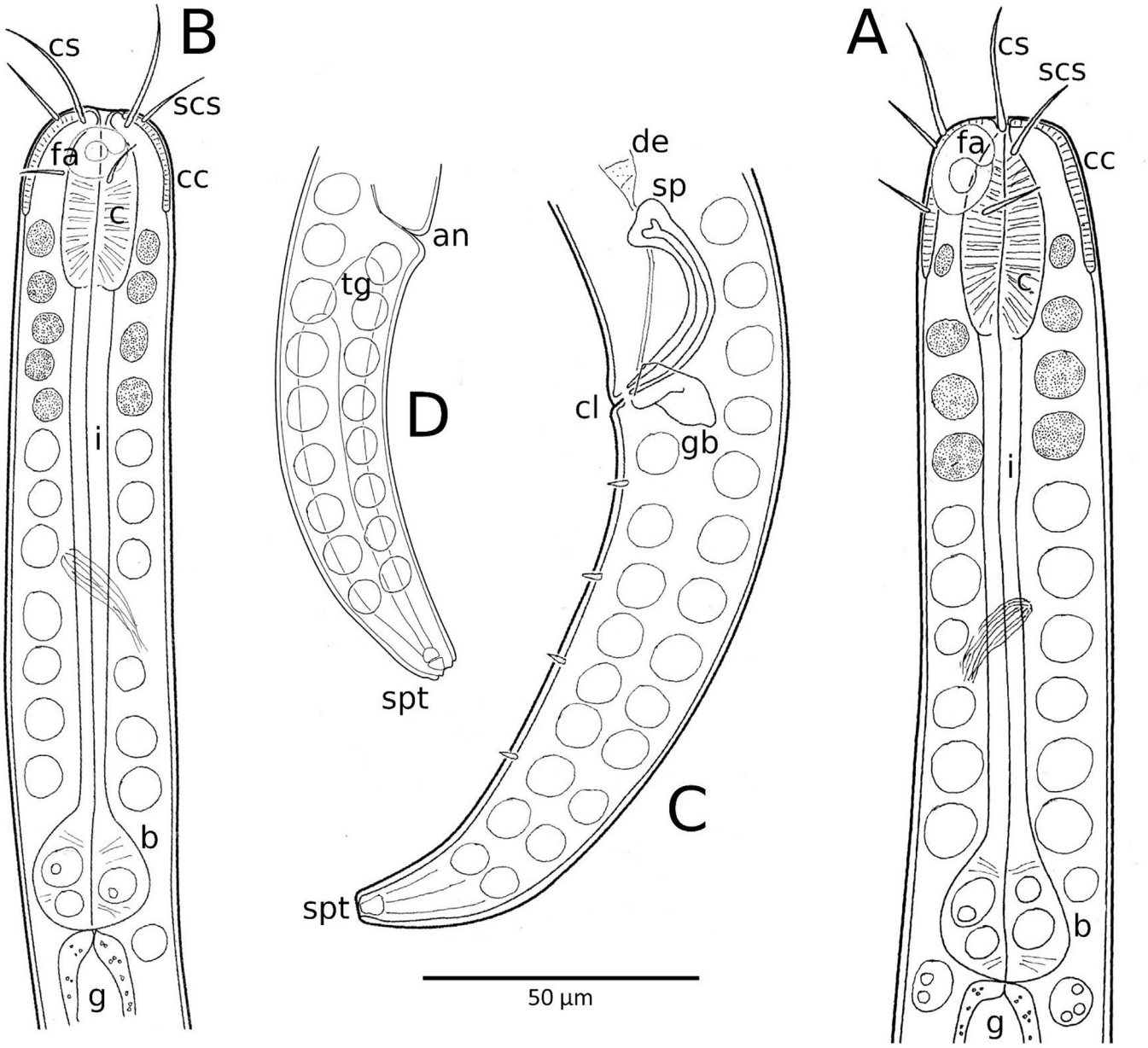

Figure 6. *Robbea weberae* sp. nov.. A, pharynx region of male holotype. B, pharynx region of female paratype.. C, tail region of male holotype. D, tail of female paratype. Abbreviations: anus, an; bulbus, b; begin bacterial coat, bbac; corpus, bbac; cephalic capsule, cc; cloaca, cl; cephalic seta, cs; ductus ejaculatorius, de; enlarged glandular sense organs, egso; fovea amphidialis, fa; gut, g; gubernaculum, gb; isthmus, i; subcephalic seta, scs; spiculum, sp; spinneret, spt; testis, t; tail gland, tg.

Small (L < 6 mm) and stouter than the forgoing species (a < 160), cephalic capsule 65% of corpus length, subcephalic setae 64% of cephalic setae, corpus less than 25% of pharynx (Figure 15).

Robbea sp. Red Sea

Sampling locations: Dahab, Egypt—Eel Garden, 28.505306 N, 34.521889 E and Marsa Alam, Egypt—Sharm Luli, 24.610056 N, 35.113583 W.

Material: One male and one female from each sampling location, in the collection of J.A. Ott.

Description: With the characters of the genus, measurements see Supporting Information, Table S2 (excel sheet).

The four specimens probably do not belong all to the same species. The male from Dahab is much longer (L > 8 mm) and more slender (a >> 200) than the remaining three individuals (Figure 16). Its cephalic capsule is short (<60% of corpus length), its subcephalic setae are long (75% of cephalic setae). The enlarged ventral GSO in the post-pharyngeal region protrude as 21 bumps. In contrast the male from Marsa Alam does not show protruding bumps. It shares with both females a shorter body length (L < 6 mm), a stouter shape (a < 190), a longer cephalic capsule (>70% of corpus length), and shorter subcephalic setae.

Robbea sp. Great Barrier Reef

Sampling location: Lizard Island, Great Barrier Reef, Australia; intertidal, medium sand. Coordinates: 14.693 S, 145.460 E.

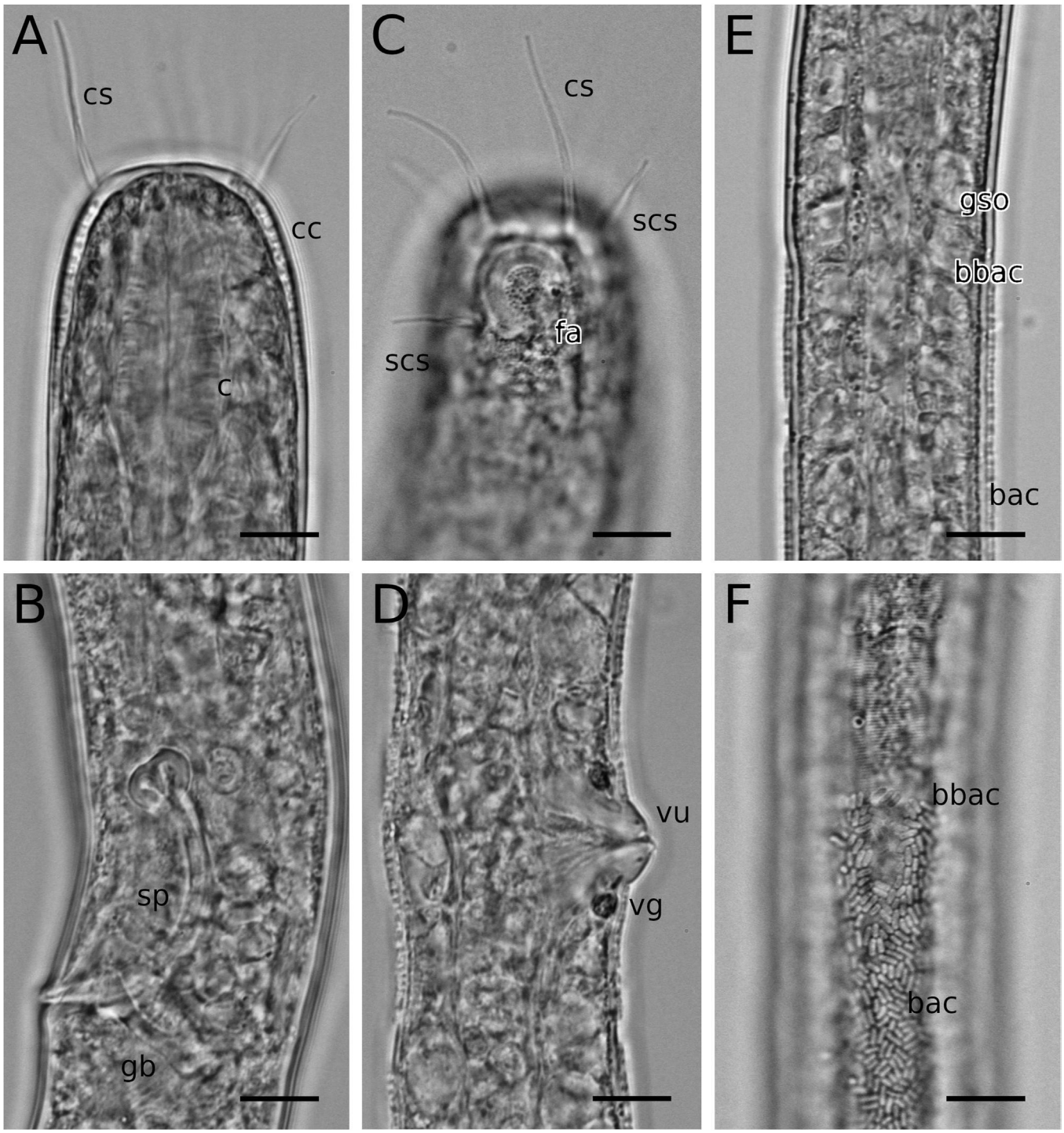

Figure 7. *Robbea weberae* sp. nov.. A, anterior end of male holotype, optical section. B, spicular apparatus of holotype. C, anterior end of paratype, surface view. D, vulva, female paratype. E, beginning of bacterial coat, optical section. F, beginning of bacterial coat, surface view. LM of preserved specimens. Abbreviations: symbiotic bacteria, bac; beginning of bacterial coat, bbac; corpus, c; cephalic capsule, cc; cephalic seta, cs; fovea amphidialis, fa; gubernaculum, gb; subcephalic seta, scs; spiculum, sp; vulvar gland, vg; vulva, vu. Scale bars: A–F, 10 µm.

Material: Two male, one female specimens in the collection of J.A. Ott.

Description: With the characters of the genus, measurements see Supporting Information, Table S2.

Small (L <= 6 mm) species (Figure 17); the three specimens vary strongly in several measurements, e. g. a (150–180), relative length of subcephalic setae (40–60% of cephalic setae length), proportions of the pharynx divisions (corpus 27–38%, isthmus 45–60% of pharynx length).

The genus *Cyathorobbea* gen. nov.

Genus diagnosis

Stilbonematinae; body stout (a < 110), cuticle finely striated, cephalic capsule with block layer; first circle of cephalic sense organs as

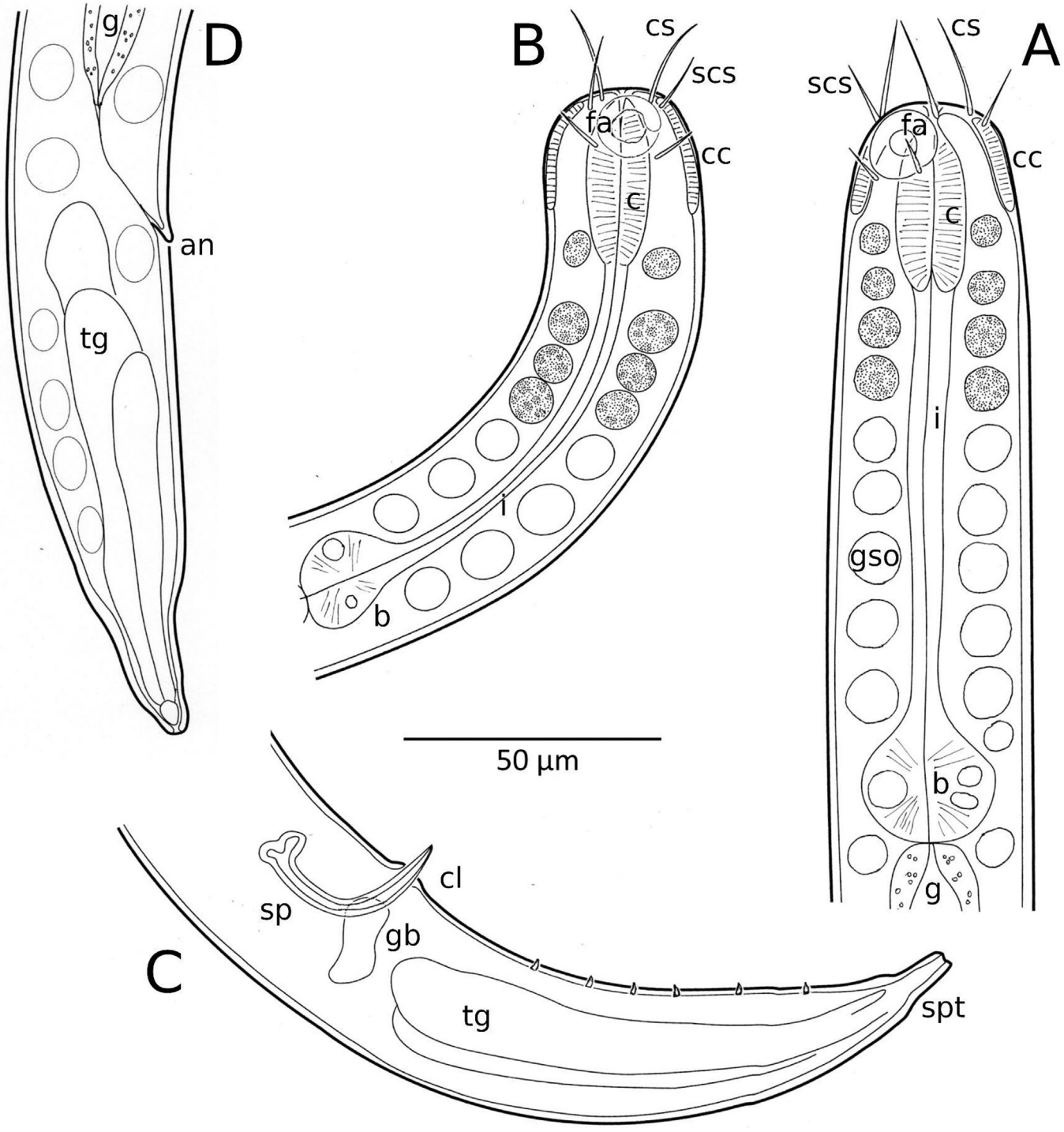

Figure 8. *Robbea lotti* sp. nov. A, pharynx region of male holotype. B, pharynx region of female paratype C, tail region of male holotype. D, tail of female paratype. Abbreviations: anus, an; bulbus, b; corpus, c; cephalic capsule, cc; cloaca, cl; cephalic seta, cs; fovea amphidialis, fa; gut, g; gubernaculum, gb; isthmus, i; subcephalic seta, scs; spiculum, sp; spinneret, spt; testis, t; tail gland, tg.

six finger-like papillae retracted into mouth opening, second circle as six conical papillae (<1 µm long) at margin of buccal membrane in lateral and submedian position; four long cephalic setae in sublateral position, directed anteriorly, close to the anterior margin of the amphidial fovea; two or three circles of eight subcephalic setae each, with four in submedian position and four sublateral, the first close to the cephalic setae. Somatic setae present, of variable length; GSOs colourless, in eight rows, two sublateral rows on each side and two submedian rows dorsally and ventrally, respectively. Amphidial fovea variable in shape, with spiral or loop-shaped groove, ventrally wound pharynx with strongly swollen muscular corpus, distinctly set off from the isthmus, terminal bulbus mainly glandular. Spicula curved, cephalate, capitulum not heart-shaped, gubernaculum variable in shape, with or without apophysis; males with ventral row of 11–19 sucker-like supplements in post-pharyngeal region, tail conical or cylindro-conical.

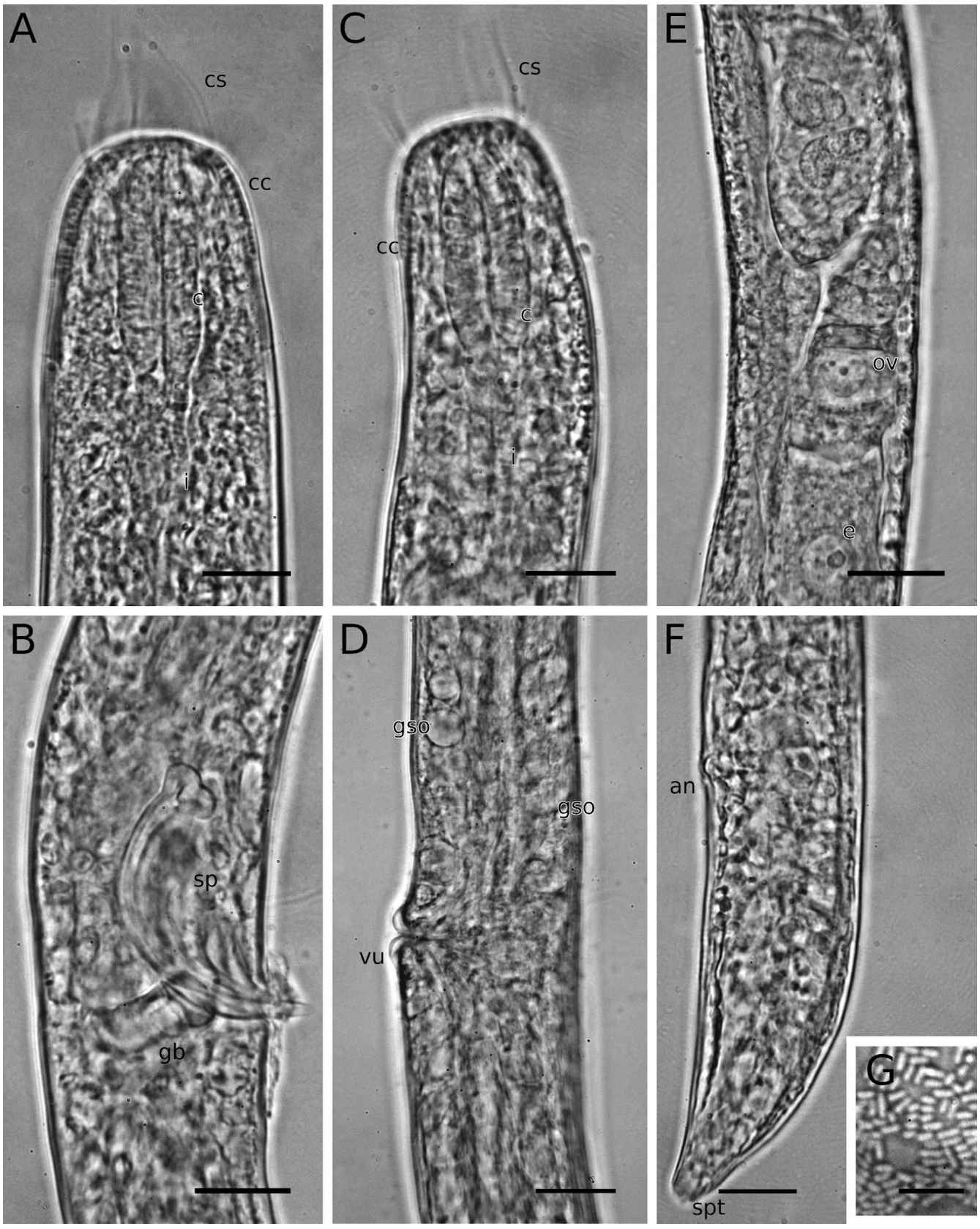

Figure 9. *Robbea lotti* sp. nov.. A, anterior end of male holotype, optical section. B, spicular apparatus, holotype. C, anterior end of female paratype, optical section. D, vulva, female paratype. E, anterior ovary, paratype. F, tail, female paratype. G, symbiotic bacteria on body surface. LM of preserved specimens. Abbreviations: anus, an; corpus, c; cephalic capsule, cc; cephalic seta, cs; egg, e; gubernaculum, gb; isthmus, i; ovary, ov; spiculum, sp; spinneret, spt; vulva, vu. Scale bars: A, B, C, E, F, 15 μm; D, 20 μm; G, 10 μm.

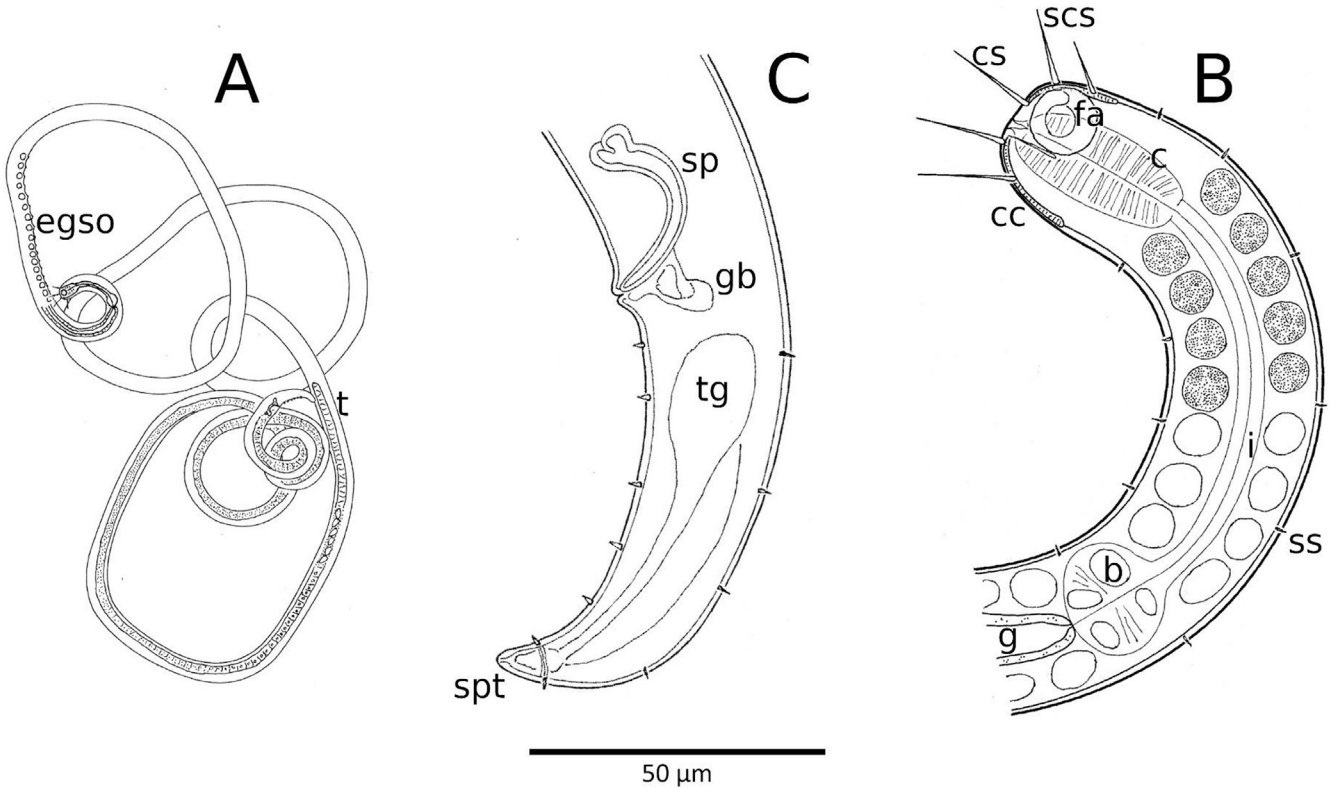

Figure 10. *Robbea seahi* sp. nov.. A, total view of holotype. B, pharynx region of holotype. C, tail region of paratype. Abbreviations: bulbus, b; corpus, c; cephalic capsule, cc; cephalic seta, cs; enlarged glandular sense organs, egso; fovea amphidialis, fa; gut, g; gubernaculum, gb; isthmus, i; subcephalic seta, scs; spiculum, sp; spinneret, spt; somatic seta, ss; testis, t; tail gland, tg.

Dense monolayer of ectosymbiotic rods or coccobacilli attached to the cuticle, starting at the posterior margin of the cephalic capsule or at a distance from the anterior end to near tip of tail. In most species, bacteria arranged with their longer axis perpendicular to the nematode's cuticle, divide longitudinally (see Fig. 18 for host and symbiont characteristics).

List of species

- *Cyathorobbea tenax* nov. comb. (type species)
  Syn: *Robbea tenax* Gerlach 1963
- *Cy. hopperi* nom. nov.
  Syn: *R. tenax* in Hopper and Cefalu 1973
- *Cy. hypermnestra* nov. comb.
  Syn: *R. hypermnestra* Ott *et al.* 2014
- *Cy. ruetzleri* nov. comb.
  Syn: *R. ruetzleri* Ott *et al.* 2014
- *Cy. agricola* nov. comb.
  Syn: *R. agricola* Ott *et al.* 2014

Remarks: The taxonomic position of *Robbea gerlachi* Boucher 1975 is uncertain. The second circle of long subcephalic setae and the value of a < 110 suggests a placement within *Cyathorobbea*; the shape of the head, however, is similar to *Robbea* species. Since the species is known from preserved females and juveniles only, the decisive character of the sucker-like supplements in males cannot be determined. The specimen described as *Robbea tenax* in Hopper and Cefalu (1973) differs in morphometric characteristics from the original description by Gerlach, 1963 (see PCA, Fig 19). We therefore propose it to be a different species and assign it the name "*hopperi*".

Interspecies similarities in the genus *Robbea* that require multivariate analysis of morphological data

Species of the genus *Robbea* are difficult to distinguish using single morphological characters. We, therefore, used a principal component analysis (PCA), based on 14 morphological characters, to separate the species from each other (Fig. 4A). In addition, we included all previously well-described *Robbea* species, where no molecular data were available, as well as all *Cyathorobbea* gen. nov. species into the analysis. Our analysis clearly separated all species of *Cyathorobbea* gen. nov. from *Robbea*, thus supporting the placement into two different genera (Fig. 19A). Within the genus *Robbea*, those species, for which multiple individuals were available for the analysis (*R. judithae* sp. nov., *R. seahi* sp. nov., *R. weberae* sp. nov., and *R. lotti* sp. nov.), showed a distinct separation from each other (Fig. 19). Especially for the latter two species, this was highly relevant; they co-occur in the same habitat, show overlap in morphological markers, and their specific nature would have gone undetected if it were not for the combination of both the molecular analysis and the multivariate morphological approach. For the genus *Robbea* that has the largest number of species with multiple specimens, we furthermore compared our morphometry-based phylogeny with the 18S rRNA marker gene-based phylogeny (Fig. 19B) and both phylogenies resolved the same species-level groupings, but they differed in the arrangement of the deeper nodes, representing the relationships of the species to each other.

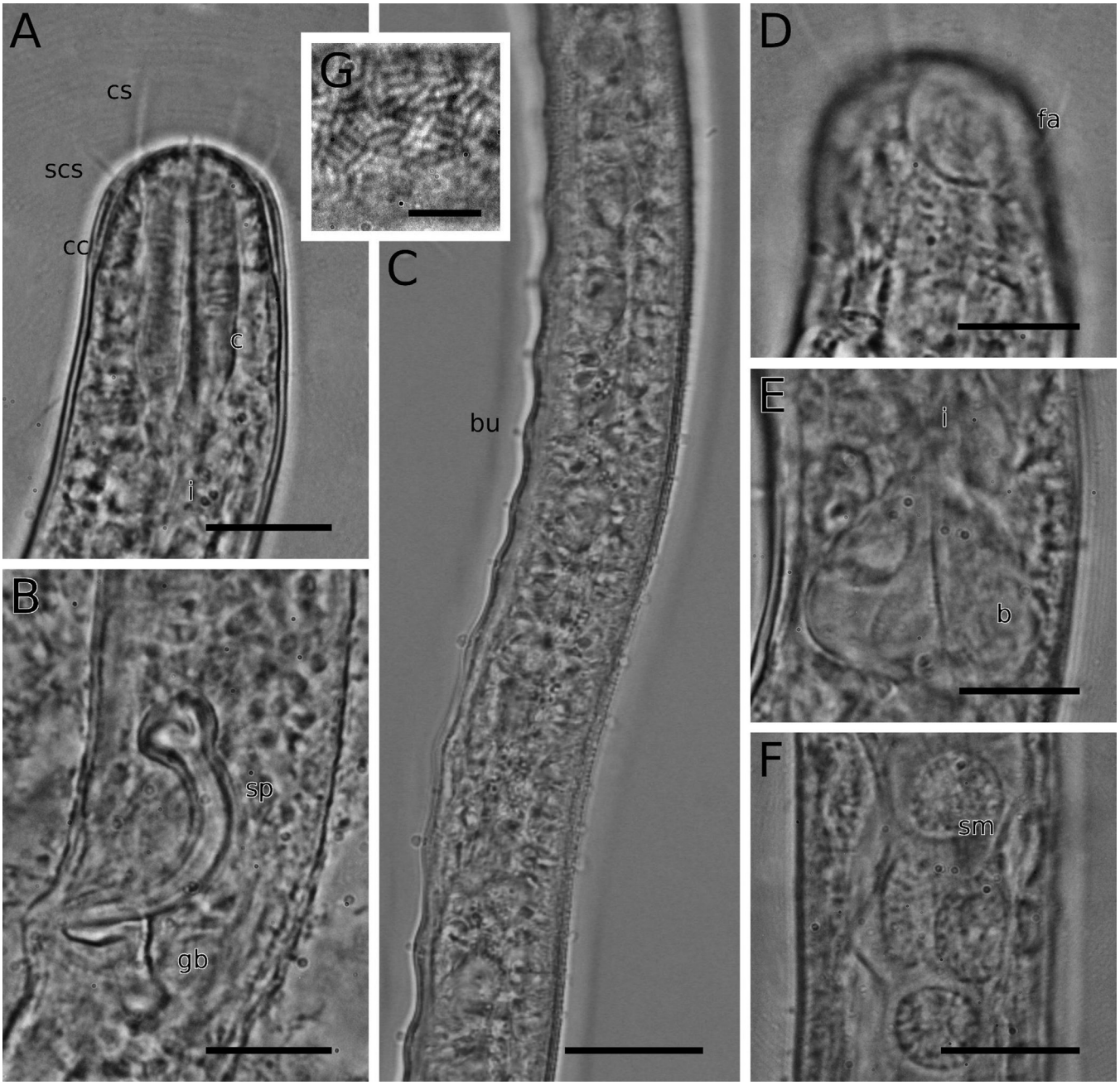

Figure 11. *Robbea seahi* sp. nov.. A, anterior end of holotype, optical section. B, spicular apparatus of holotype. C, post-pharyngeal region of holotype. D, anterior end of paratype, surface view. E, pharynx bulbus of paratype. F, sperm in paratype. G, symbiotic bacteria on body surface. LM of preserved specimens. Abbreviations: bump, bu; corpus, c; cephalic capsule, cc; cephalic seta, cs; gubernaculum, gb; isthmus, i; ovary, ov; spiculum, sp. Scale bars: A, B, F, 15 μm; D, E, 10 μm; C, 25 μm; G, 15 μm.

Host and symbiont marker gene phylogenies corroborate the distinction of the two genera *Robbea* and *Cyathorobbea* gen. nov.

For a wider phylogenetic context, and to clarify the relationship of *Robbea* and *Cyathorobbea* to each other and within the Stilbonematinae, we performed molecular identification for all new species described in this paper, using the host 18S rRNA and the mitochondrial *COI* gene and the symbionts' 16S rRNA gene. For the hosts, both the 18S rRNA- and the *COI*-gene analyses showed that all new *Robbea* species form a distinct and highly supported genus-level clade, separate from all published *Cyathorobbea* sequences, and each species in this clade is supported as well (Fig. 20A, B).

The 18S sequences of the species that we assigned to the new genus *Cyathorobbea*, namely *Cy. hypermnestra*, *Cy. ruetzleri*, and *Cy. agricola*, formed a highly supported clade, independent of the genus *Robbea*. The same clustering was observed in the *COI* phylogeny. Overall, both marker gene analyses corroborate *Robbea* and *Cyathorobbea* as two different genera within the Stilbonematinae (see Fig. 20A, B; Supporting Information, Figs S1, S2).

Our 16S rRNA-based phylogenetic analysis of the ectosymbionts associated with *Robbea* and *Cyathorobbea* showed

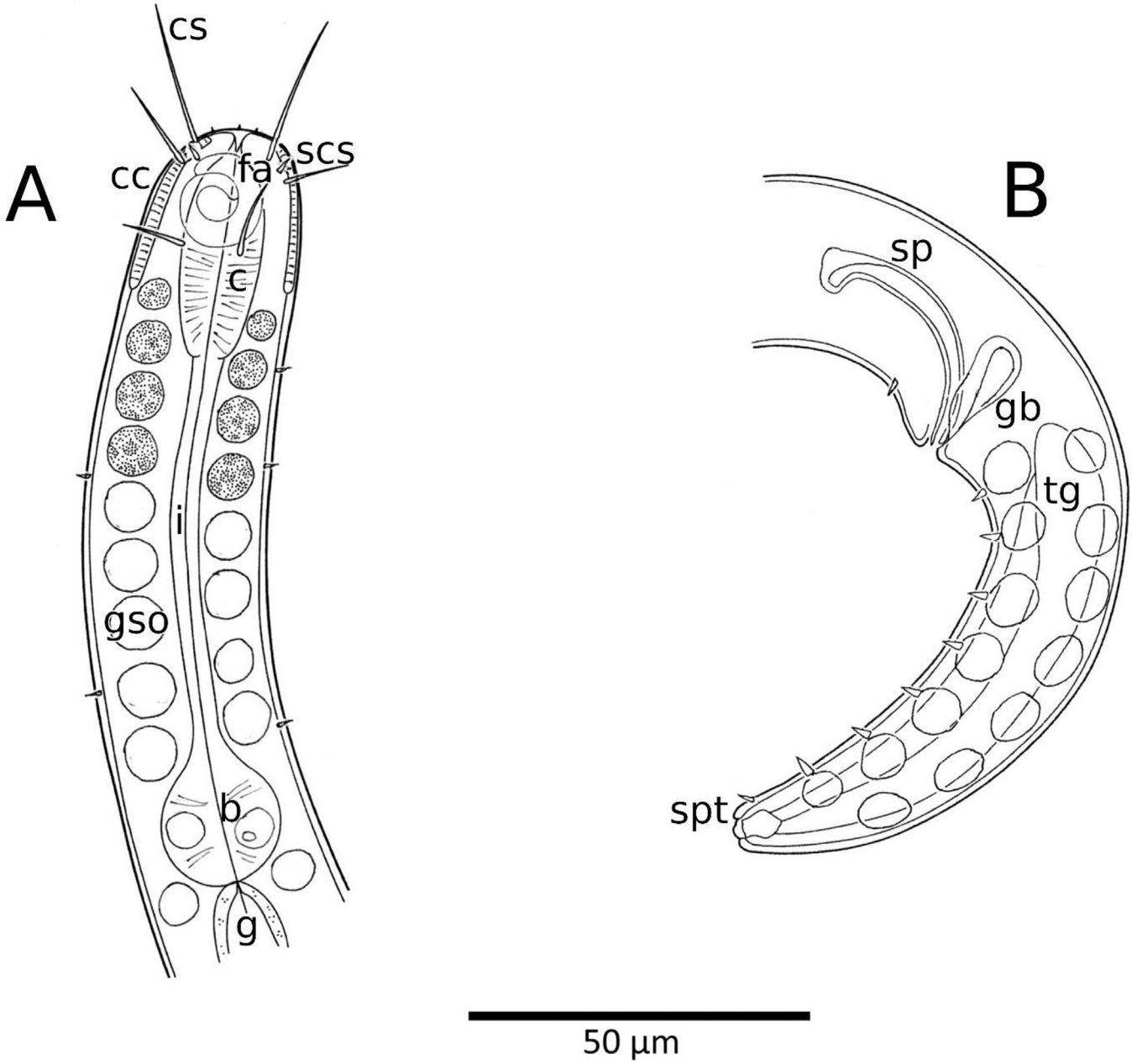

Figure 12. *Robbea bernarditae* sp. nov.. A, pharynx region of holotype. B, tail region of holotype. Abbreviations: bulbus, b; corpus, c; cephalic capsule, cc; cephalic seta, cs; fovea amphidialis, fa; gut, g; gubernaculum, gb; isthmus, i; subcephalic seta, scs; spiculum, sp; somatic seta, ss; tail gland, tg.

two highly supported clades within *Candidatus* Thiosymbion that corresponded to the two host genera (see Supporting Information, Fig. S3). Within the general *Robbea* ectosymbiont clade, all sequences form sub-clades mirroring their host species' clades. Similarly, all 16S rRNA sequences of the symbionts of the *Cyathorobbea* clade form a distinct and independent genus-level clade that is structured according to the host species. This highlights the differences between the *Robbea* and *Cyathorobbea* genera on the holobiont level.

Geographic distribution of *Robbea* and *Cyathorobbea*

Species of the genus *Robbea* are found in all major ocean basins. In contrast, *Cyathorobbea* species are so far only reported from the tropical West Atlantic and the Indian Ocean (Fig. 1C). The latitudinal distribution of the genus *Robbea* is exceptionally wide, ranging from 57°50′N at Loch Ewe (Scotland) to 14°40′S at Lizard Island, Australia. (Fig. 1C). Except for a record of *Leptonemella aphanothecae* Gerlach 1950 from the White Sea by Tchesunov (2013), the Scottish findings are the most northern reports of any Stilbonematinae to date.

The marine nematode genus *Robbea* carries large inclusions within its glandular sense organs.

All live specimens of *Robbea* in this study showed a dark coloration throughout the body. The colour was localized inside the GSOs in the form of dark, round structures with coloration ranging from

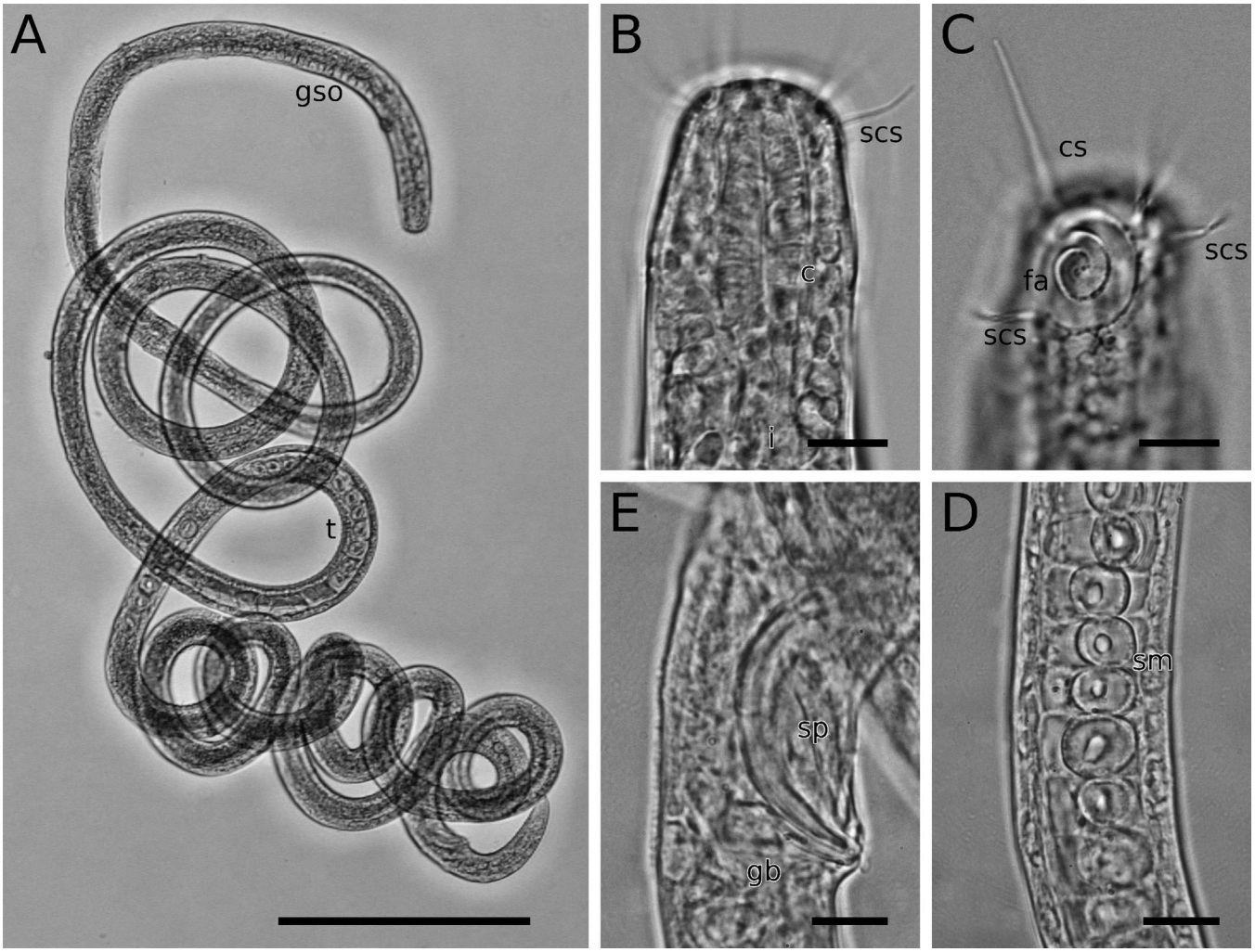

Figure 13. *Robbea bernarditae* sp. nov.. A, total view of holotype. B, anterior end, holotype, optical section. C, anterior end, holotype, surface view. D, sperm, paratype. E, spicular apparatus, holotype. LM of preserved specimens. Abbreviations: corpus, c; cephalic seta, cs; fovea amphidialis, fa; gubernaculum, gb; isthmus, i; subcephalic seta, scs; sperm, sm; spiculum, sp; testis, t. Scale bars: A, 200 μm; B, C, E, 10 μm; D, 15 μm.

dark blue to olive brown (Fig. 21A–D). In both aldehyde- and ethanol-fixed specimens, the colour disappeared over time.

Micro-CT scans of a specimen of *Robbea judithae* sp. nov. revealed 4747 electron-dense inclusions ranging in size from 0.017 to 378.7 μm^3 that, in total, made up 2.25% of the nematode's volume. Many of these inclusions, and especially the larger size ranges, showed the same distribution as the dark structures inside the GSO, the largest being in the body regions anterior and posterior to the gonads (Supporting Information, Figs S4 and S5). In serial sections of the specimen used for the μCT analysis, the inclusions were visible as olive green granules inside the GSO in light microscopy. Correlative TEM sections confirmed the location of the granules (Fig. 21E–G). Whether these inclusions are within the cells of the GSOs or extracellularly between the cells, cannot be confirmed at this stage. The seemingly crystalline nature of the inclusions leads to compression and breakage when sectioning them, indicated by the white halos around them in Fig. 21G.

The inclusions contain bromide and iron

To identify the cause of the coloration of the GSOs, we used energy dispersive X-ray analyses (EDX) on whole nematodes from two different geographic locations and two different stilbonematine genera. We detected concentrated and overlapping signals for bromide and iron in all specimens ($N = 8$) of the genus *Robbea*, independent of their sampling location (Fig. 22). The bromide and iron signals corresponded in location, shape, and size with the inclusions found in the μCT and LM analyses (Fig. 21). As a control, we performed EDX on two different species of the closely related stilbonematine genus *Catanema*, sampled from the same sampling location as *Robbea* in Belize (Catanema sp. '*thin*', $N = 4$), as well as from the Mediterranean (*Catanema schiemeri*, $N = 4$). Neither of them showed any dark coloration in GSOs and, correspondingly, no iron or bromide was detected (Fig. 22).

Taken together, our correlative microscopy and EDX data indicate that the dark coloration of these newly described members of the genus *Robbea* is caused by high amounts of iron and bromide, which are contained in inclusions in the GSOs.

DISCUSSION

The genera *Robbea*, *Catanema*, and *Cyathorobbea*

Since its erection by Gerlach, with the description of *R. caelestis* (1956) based on a specimen from Brazil, several species have

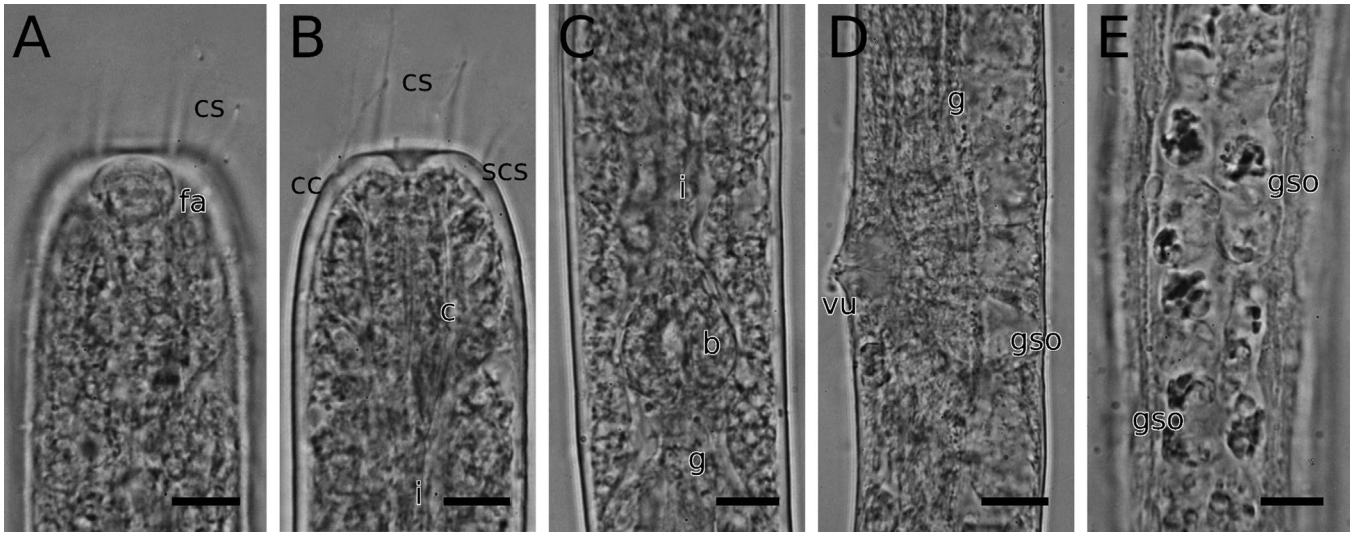

Figure 14. *Robbea* sp. Bahamas. A, anterior end, female, surface view. B, nterior end, female, optical section. C, pharynx bulbus. D, vulva. E, midbody region with pigmented GSOs. LM of preserved specimens. Abbreviations: bulbus, b; corpus, c; cephalic capsule, cc; cephalic seta, cs; fovea amphidialis, fa; gut isthmus, i; ovary, ov; subcephalic seta, scs; vulva, vu. Scale bars: A, B, C, E, 10 μm; D, 15 μm.

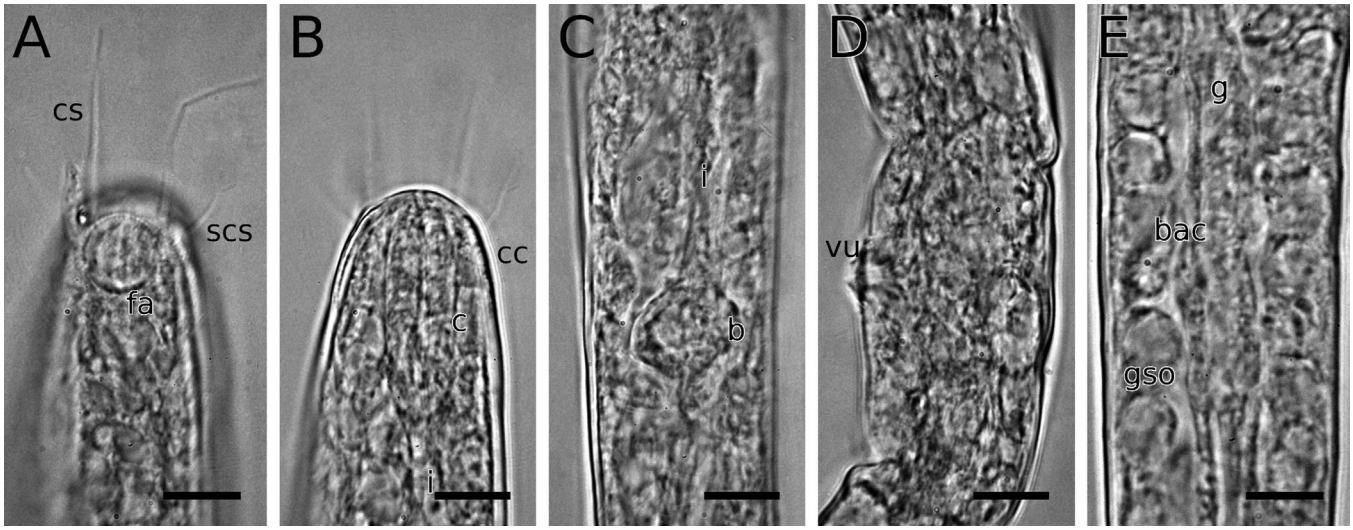

Figure 15. *Robbea* sp. Bermuda. A, anterior end, female, surface view. B, anterior end, female, optical section. C, pharynx bulbus. D, vulva. E, midbody region with GSO and bacteria in gut lumen. LM of preserved specimens. Abbreviations: bulbus, b; bacteria, bac; corpus, c; cephalic capsule, cc; cephalic seta, cs; fovea amphidialis, fa; gut, g; subcephalic seta, scs; vulva, vu. Scale bars: A–E, 10 μm.

been placed into the genus *Robbea*. Already when describing the second species, *R. tenax* from the Maldives, Gerlach (1963) was aware of the profound differences between the two species; however, the peculiar anatomy of the pharynx seemed to justify their congeneric status. Mostly based on pharyngeal characters, the genus *Robbea* was then synonymized with the genus *Catanema* (Platt and Zhang 1982) but later was re-defined by Tchesunov (2013), who placed all species with spiral amphids and muscular corpus in the genus *Robbea* (including *Catanema porosum*).

Armenteros *et al.* (2014a, b) reported *Robbea porosum* (Hopper and Cefalu 1973) from Cuba and raised concerns about the monophyletic status of the genus *Robbea*. Differences to the original description as *Catanema porosum*—such as the more slender body, the shorter pharynx, and the much shorter cephalic and subcephalic setae—became especially apparent in our multivariate analysis of morphological characters and suggested that it represented a different species (see Fig. 19, *Robbea* sp. 'Cuba'). Furthermore, when providing partial 18S and *COI* sequences, the authors were already aware that these sequences appear to belong to two distinct species. Unfortunately, these sequences cannot unequivocally be assigned to the specimens measured and illustrated in Armenteros *et al.* (2014b). In our analysis, the sequence designated by Armenteros and co-workers as ND007 (18S rRNA) and ND007, ND005, and ND043 (*COI*) cluster with a specimen known from sequencing only (designated here as *R.* sp. 'Belize2') in the respective gene trees. The sequences labelled ND014 (18S rRNA) and ND008, ND014, and ND040 (*COI*), however, cluster with *Robbea lotti* from Elba (Supporting Information, Figs S1, S2).

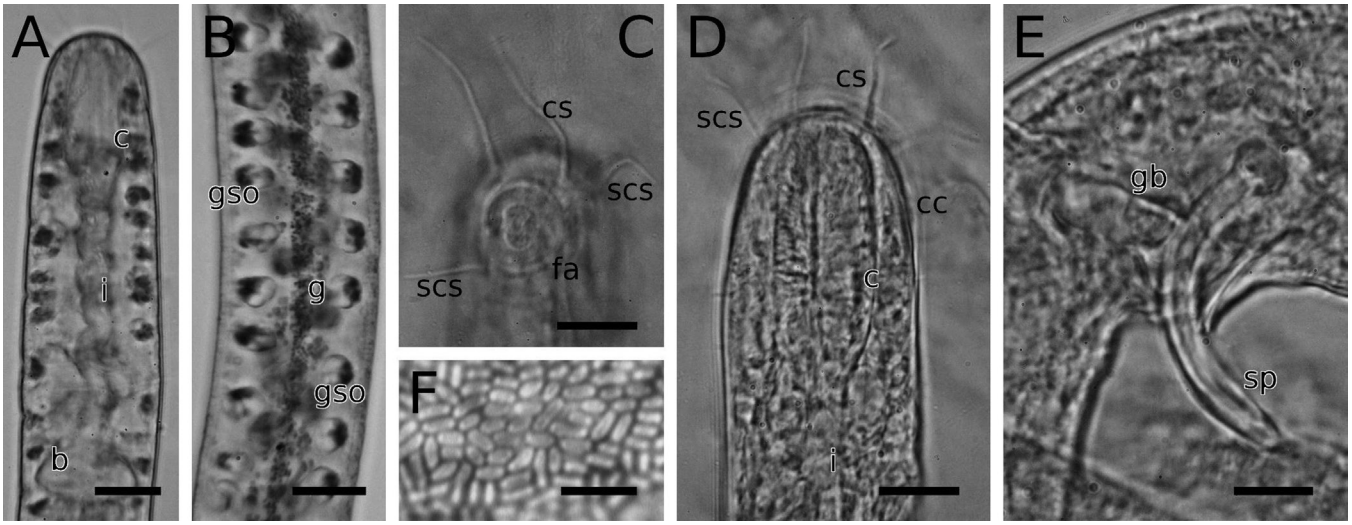

Figure 16. *Robbea* sp. Red Sea. A, pharyngeal region. B, midbody region. C, anterior end, male from Marsa Alam, surface view. D, anterior end, female from Dahab, optical section. E, spicular apparatus, male from Dahab. F, symbiotic bacteria on body surface. A, B, LM of live specimens; C–F, LM of preserved specimens. Abbreviations: bulbus, b; corpus, c; cephalic capsule, cc; cephalic seta, cs; fovea amphidialis, fa; gut, g; gubernaculum, gb; isthmus, i; subcephalic seta, scs; spiculum, sp. Scale bars: A, B, 15 μm; C, D, E, 10 μm; F, 5 μm.

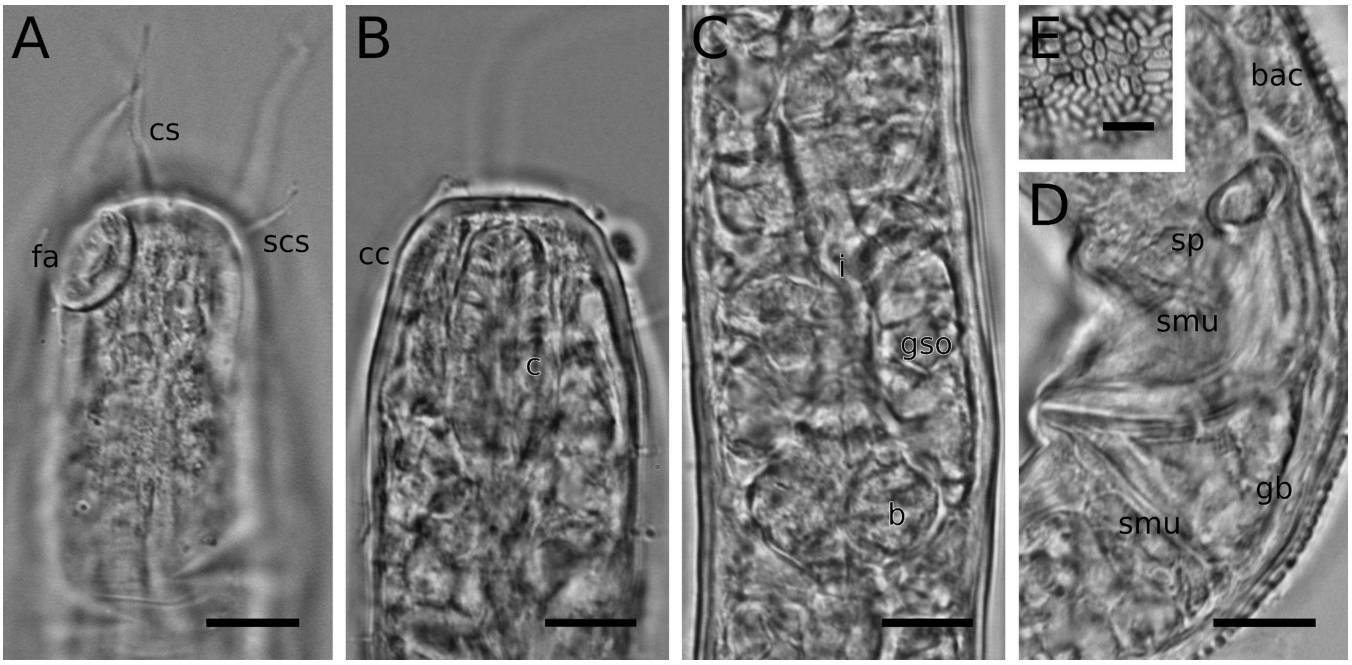

Figure 17. *Robbea* sp. Great Barrier Reef. A, anterior end of male, surface view. B, anterior end of male, optical section. C, pharynx bulbus. D, spicular apparatus. E, symbiotic bacteria ;on body surface. LM of preserved specimens. Abbreviations: bulbus, b; bacteria, bac; corpus, c; cephalic capsule, cc; cephalic seta, cs; fovea amphidialis,fa; gubernaculum, gb; isthmus, i; subcephalic seta, scs; muscles of the spicular apparatus, smu; spiculum, sp. Scale bars: A–D, 10 μm; E, 5 μm.

Our analyses of the black-dotted nematodes of the genus *Robbea* showed that they are molecularly different from any of the previously described Central American species previously assigned to the genus *Robbea* (Figs 19, 20). This allowed an emended morphological genus definition for *Robbea* Gerlach 1956, with *R. caelestis* as the type species, and the erection of the novel genus *Cyathorobbea* with *C. tenax* as the type species.

Support of the genera from symbiont phylogeny

All the newly described *Robbea* species carry host-species' specific ectosymbionts. The remarkably high host specificity of *Candidatus* Thiosymbion is typical for stilbonematine nematodes and in stark contrast to the closely related *Ca*. Thiosymbion symbionts of gutless oligochaetes, where host switching and uptake of locally adapted bacterial symbionts can occur (Zimmermann *et al.* 2016, Mankowski *et al.* 2021). As previously reported for stilbonematine nematodes, the arrangement of the bacterial coat on the cuticle is specific to their host genus (Scharhauser *et al.* 2020). The symbionts of the newly described *Robbea* species are no exception to this. In both genera, the symbiont coat starts posterior to the pharynx. While all species of *Robbea* have rod-shaped symbionts that are in contact with the

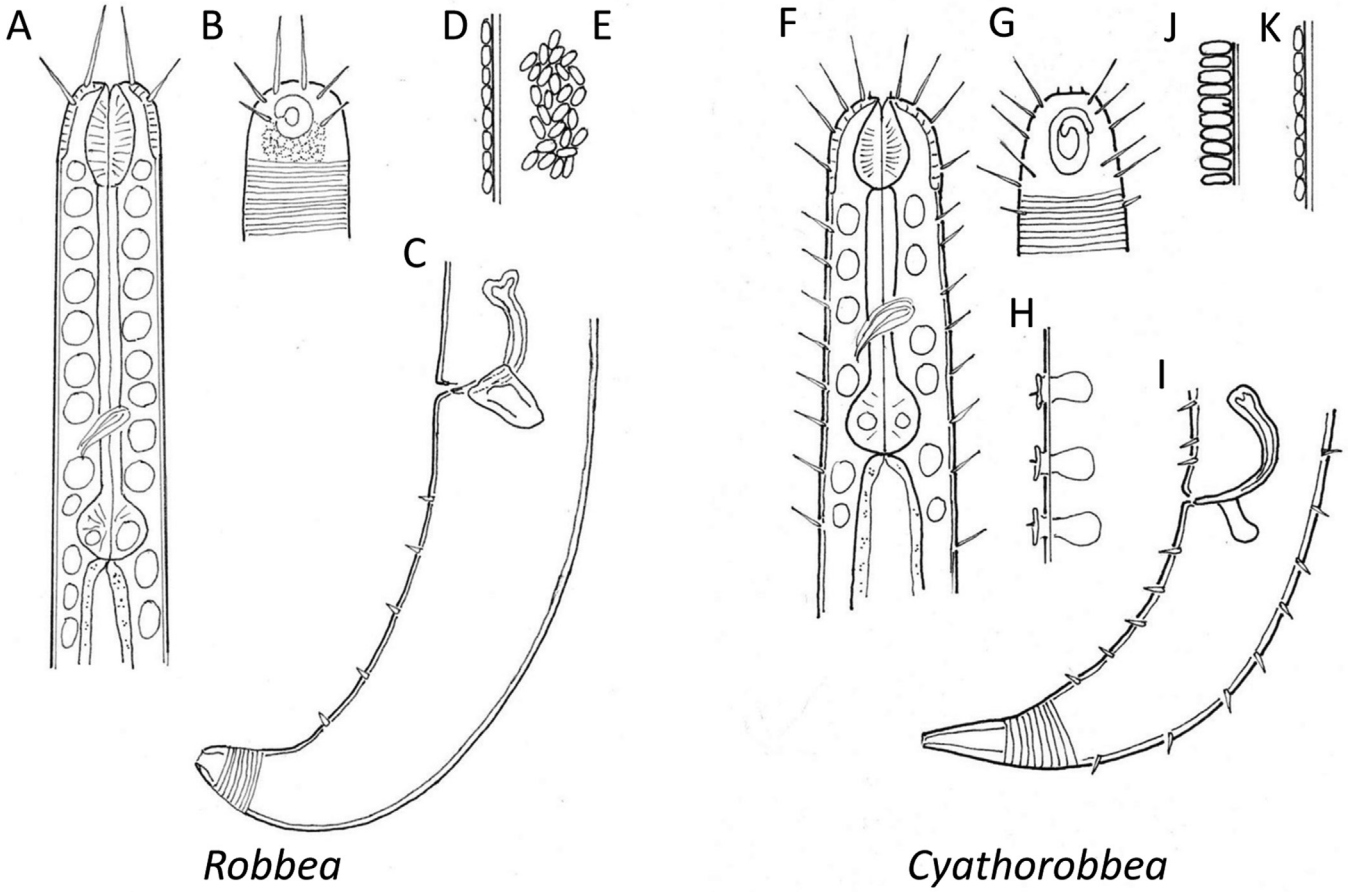

Figure 18. Schematic representation of the characteristics of the genera *Robbea* and *Cyathorobbea*. A–E, *Robbea*. A, anterior body region. B, surface view of head region. C, posterior end of male. D, symbiotic bacteria in optical section. E, surface view. F–K, *Cyathorobbea*. F, anterior body region. G, surface view of head region. H, cup-shaped (cyathiform) male supplements. I, posterior end of male. J, K, optical sections of the two types of bacterial arrangements.

cuticle along their longitudinal axis (Figure 18D), some species of the genus *Cyathorobbea* deviate from this and carry rod-shaped bacteria that are standing upright, with only their cell pole in contact with the cuticle and the cells dividing longitudinally (Fig. 18, J, K; Table 1; Leisch *et al.* 2016).

The power of standardized vouchering and morphometric analyses

The realization that apparently morphologically indistinguishable species are genetically distinct has wide-ranging implications beyond species' descriptions, impacting our understanding of biodiversity, mutualistic interactions, and conservation efforts, to name a few (reviewed in: Bickford *et al.* 2007). In Stilbonematinae their obligate symbiosis with bacteria has been suggested as a cause for stabilizing selection, which in turn could result in cryptic speciation (Armenteros *et al.* 2014b). However, given that some genera of Stilbonematinae can easily be distinguished into species, whilst other genera show a large number of highly similar species, the symbiotic association might be only one of several and potentially non-exclusive explanations. Overall, a better understanding of the morphology, the micro-niches within their habitat, the distribution of the nematodes throughout the micro-niches, and the chemosensory cues is needed to gain a better understanding of the convergence or the stability of characters.

In the case of the *Robbea* species described here, one could have argued that the specimens could all be assigned to the same species, as no single character lends itself for an unequivocal distinction of species. However, our approach to use PCA of morphological characters enabled us to corroborate the species indicated by the molecular data. In fact, both the PCA and molecular phylogenetic analyses supported the co-occurrence of two species in the same location on Elba, originally interpreted as just one species during fieldwork. Both *R. weberae* sp. nov. and *R. lotti* sp. nov. co-occur in a homogenous subtidal sand field in 5–6 m depth in the Bay of Sant' Andrea on Elba, Italy. The data generated in the field, such as the measured variation in body length and the body length/width ratio, alone did not support a split into two species. However, the clear separation in the PCA analysis led to the realization that the slightly shorter and stouter *R. lotti* nematodes are distinct from the long and slender *R. weberae* ones in several subtle characters. Informed by the PCA analysis, the voucher photos enabled us to match the morphologically defined species to the corresponding molecular data. Our findings suggest that it is necessary to reappraise reported taxonomy and distribution of Stilbonematinae based solely on morphological data, and to employ both molecular analyses and morphometric based statistics, based on standardized voucher micrographs together as state-of-the-art taxonomy.

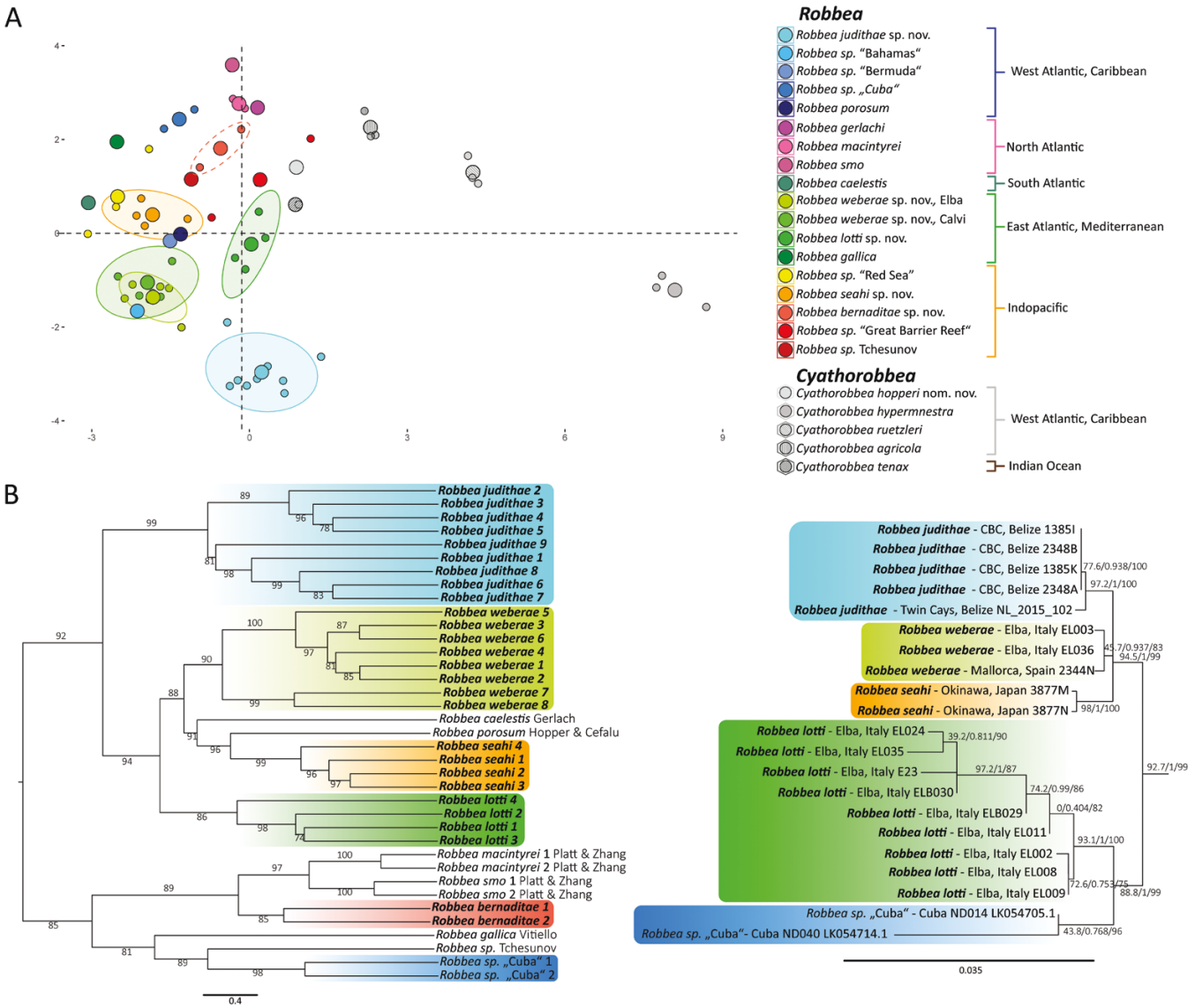

Figure 19. Specimens group according to species in molecular and morphometric analyses. A, PCA analysis of the morphometric data of all published and newly described *Robbea* and *Cyathorobbea* species. Small dots are the individual specimens, larger dots symbolize the arithmetic mean, ellipses represent the 80% confidence interval. *Robbea weberae* from Elba and Calvi were highlighted with different shading to indicate the two different sampling sites. B, The comparison of morphometry (PCA) on the left and molecular-based 18S phylogenies on the right shows the same species clades. Support values in B. for the morphometry tree are bootstrap nboot = 1000 (left) and for the 18S tree are Ultrafast Bootstrap/aBayes/aLRT (right).

Inclusions in benthic marine invertebrates of soft bottoms

Many marine invertebrates, such as bivalves, annelids, and priapulids, which inhabit soft bottoms, have intracellular electron-dense inclusions in epithelial tissues (Janssen and Oeschger 1992, Frenkiel *et al.* 1996, Windoffer *et al.* 1999, Wohlgemuth *et al.* 2007). These inclusions can range from storage compounds to the sequestration of toxic compounds that are often sulphur-based. In benthic marine nematodes, a similarly wide variety of inclusions with no, or a varying range of, coloration have been reported, which serve functions such as energy storage, sequestration of toxic compounds from the environment, or storage of indigestible material (see Table 2).

The inclusions in the genus *Robbea* stand out because they are exclusively in the genus *Robbea*, but not in any other nematodes co-occurring in the same habitat. They have been found in all live *Robbea* specimens irrespective of the geographic sampling location. Together, these two observations suggest that it is not a passive accumulation from their environment. Additionally, none of the sampling sites are known for high input of either bromide or iron. Bromide is easily available in seawater at typically a 65 mg/L concentration, which makes seawater a likely source (Morris and Riley 1966). This points to an active uptake of iron or bromide, either directly by the nematode host or via its food, which, in case of stilbonematine nematodes, would be their ectosymbiotic bacteria. It is unlikely that the ectosymbionts are the source of iron or bromide because there are no inclusions visible in TEM micrographs and no detectable EDX signal for iron or

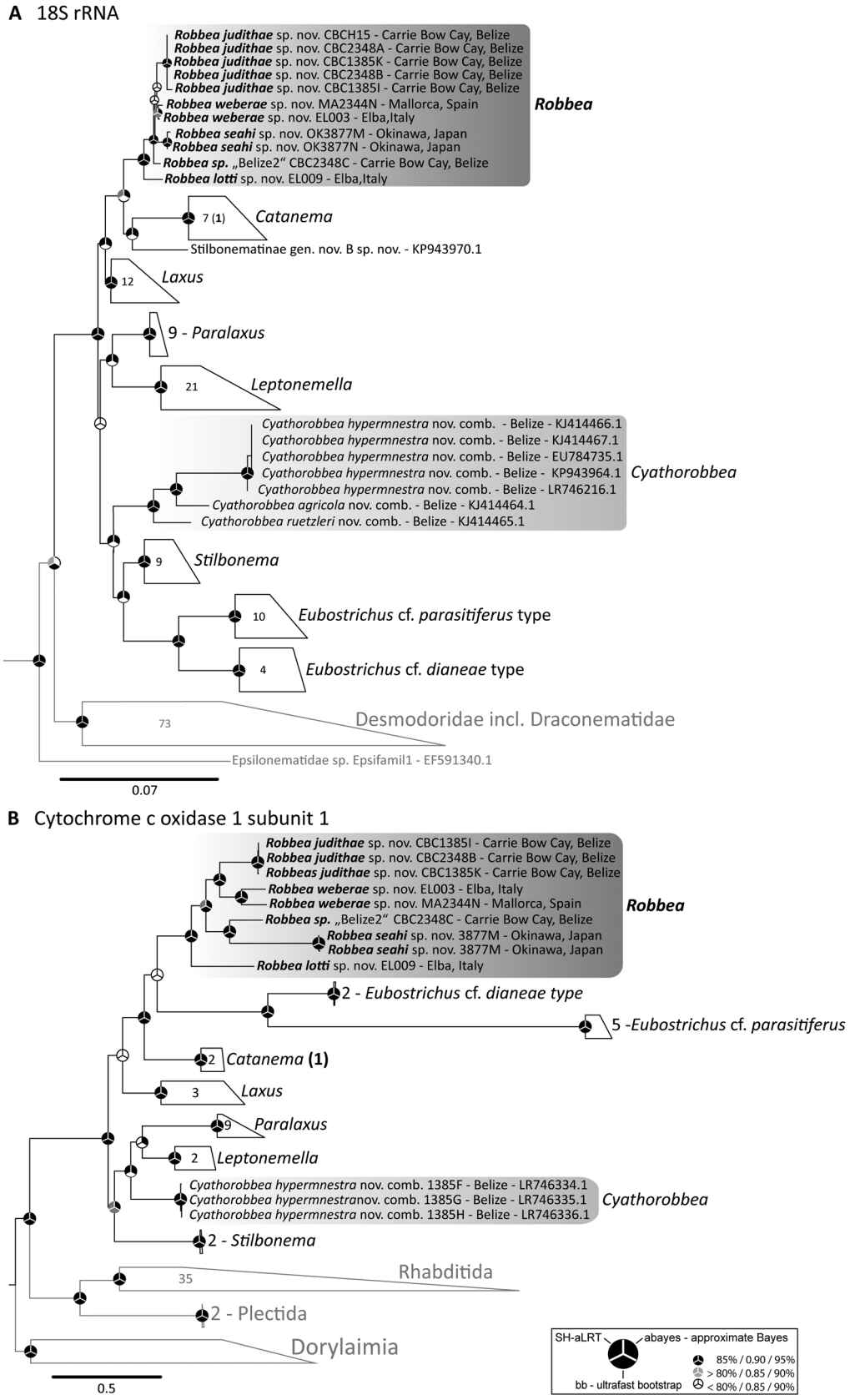

Figure 20. Ribosomal and mitochondrial gene phylogenies support *Robbea* and *Cyathorobbea* as distinct genus-level clades within the Stilbonematinae. A, phylogeny of 281 nematode 18S rRNA sequences (min. length 1300 bp), including all *Robbea* and *Cyathorobbea* sequences. Only 165 18S rRNA sequences for Desmodoroidea are shown here. The non-collapsed 18S tree is shown in Suppl. Fig.1. B, phylogeny of 83 full-length *COI* sequences of nematodes including all *Robbea* and *Cyathorobbea* species. New species and genera in this study are highlighted in bold. Provisional working name for undescribed species are given in quotes. Scale bars represent average nucleotide substitutions per site. Accession numbers for sequences from this study are listed in the Supporting Information, Table S1. Non-collapsed *COI* tree is shown in the Supporting Information, Fig. S2.

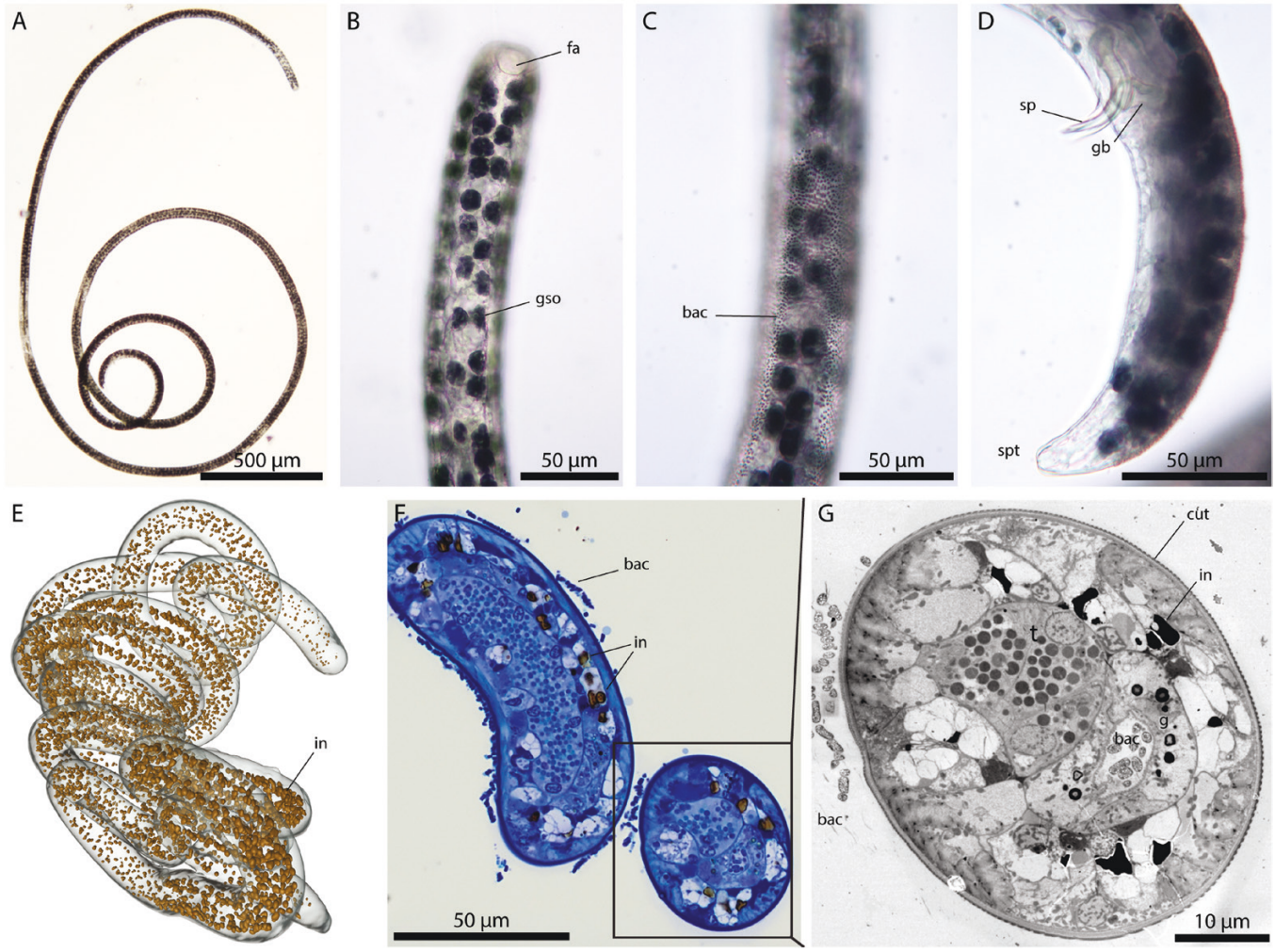

Figure 21. Inclusions in *Robbea judithae*. A, total view of live male specimen, showing dark-coloured GSOs extending throughout body. B, anterior body region showing rows of GSOs, C, surface view of midbody region, showing coat of symbiotic bacteria. D, posterior body region, showing male copulatory apparatus. E, µCT-based surface rendering of a male specimen. Inclusions were segmented and are displayed in brown (false colour). F, semithin section through testis region of same specimen stained with toluidine blue. G, EM of cross-section indicated with black box in F. A–D, light micrographs.

bromide in the ectosymbiont cells. Contrary to inclusions in other nematodes, which typically occur in epithelial tissue (e.g. gut epithelium accumulating indigestible compounds from food), in *Robbea*, the accumulations are localized in the GSOs. These glands connect to the outside via the setae and are involved in the acquisition and maintenance of the symbiotic coat via secretion of lectins and bactericidal compounds (Bulgheresi *et al.* 2006, Bauer 2012). It is, therefore, tempting to speculate that the GSOs secrete these iron–bromide compounds as well. Although the exact molecules containing iron and bromide are not known yet, one possibility is that they are used as antimicrobial substances, since many biologically produced bromide-containing compounds are known to be toxic for both prokaryotes and eukaryotes (Gribble 1999). The nematode host could use bromide-containing compounds as a mechanism to maintain and protect its ectosymbiont coat from environmental bacteria or fungi, e.g. brominated furanones are known to have a strong inhibitory effect against the formation of microbial biofilms and quorum sensing (Zang *et al.* 2009, Park *et al.* 2017). Alternatively, these bromide compounds could be a mechanism to deter predators, as it has been reported for a variety of marine animals, such as several sponges, corals, bryozoans, molluscs (different species of sea hares—*Aplysia*), and acorn worms, but also in marine plants, such as several brown algae and filamentous red algae (Gribble 1999, Paul *et al.* 2006, La Barre *et al.* 2010, Longford *et al.* 2019).

Iron is known as a key regulator in microbial infections and has been shown to play a role in animal–microbe and plant–microbe symbioses (Plessner *et al.* 1993, Schleicher and Nyholm 2011, Eickhoff and Bassler 2020, Sankari *et al.* 2022). Eukaryotic hosts have strategies to limit the bio-availability of iron, and in turn bacterial pathogens co-evolving with their hosts have developed efficient iron-sequestration strategies (Parrow *et al.* 2013). It is tempting to speculate that the iron in the inclusions might be stored in the GSOs to also supplement symbiont metabolism. From the GSOs, the iron might then be secreted via the cuticular openings that connect the GSOs and the ectosymbiont coat. An open question is still why such inclusions only occur in the genus *Robbea* but not in any of the closely related stilbonematine nematodes.

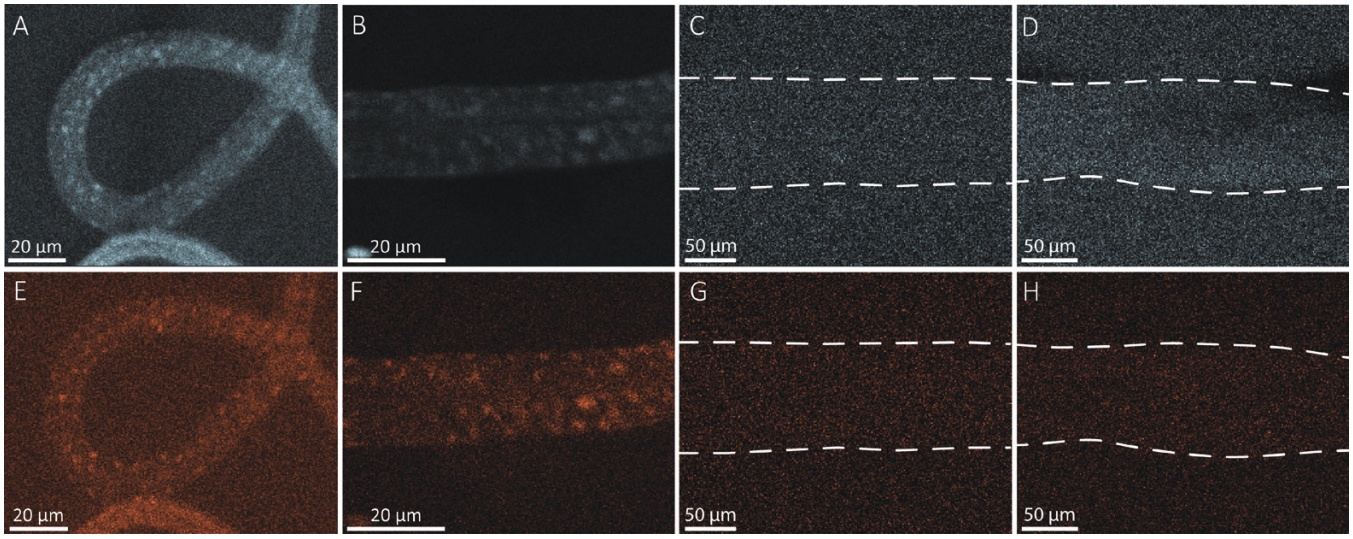

Figure 22. EDX signals of bromide (A–D) and iron (E–H) for *Robbea weberae* (A, E), *Robbea judithae* (B, F), *Catanema schiemeri* (C, G), and *Catanema* sp. '*thin*' (D, H). C, D, G, H: dashed lines indicate outline of the specimens.

Table 2. Summary of inclusions in marine nematodes

Class/Species	Location of inclusion	Chemical composition	References
Paramonohystera wieseri	Pigmentation of hypodermis	n.d.	J. Ott (1977)
Sabatiera wieseri *Terschellingia longicaudata* *Sphaerolaimus papillatus*	Chord cells in the hypodermis, the intestine and the oesophagus	Na, P, S, Cl, Fe, and Zn	Nicholas *et al.* (1987)
Eutobrilus heptapapillatus	Crystalloids in pseudocoelom	S and P	Bird *et al.* (1991)
Tripyloides marinus	Two types: - epidermal cells - intestinal syncytium	Br, Fe, and S P, Cu, and Zn	Millward (1996)
Oncholaimus campylocercoides	Two types: -intestinal cells -epidermal cells	- Fe and P - only S	Thiermann *et al.* (1994)

CONCLUSION

Character-poor groups such as nematodes are challenging for taxonomists. Often a combination of multiple characters is necessary to clearly distinguish different taxa. Our morphometric approach allowed us to use many diverse features, even from species where no sequences were available, and holds enormous potential for nematodes, as a large amount of the known diversity has been described before molecular methods became available and most of these original descriptions have sufficient morphometric data. The congruence between the morphometric and the molecular species delineations highlights that the inclusion of detailed morphological features can be highly valuable to not only separate feature-poor species, but also to bridge the gap between traditional morphological descriptions and sequencing-based approaches. A standardized morphometric analysis will enable researchers in the field to identify even feature-poor animals under the microscope, opening the doors for experiments in the field setting, or the development of machine-learning approaches for identification.

In this study we identified Fe–Br inclusions inside the GSOs and used them as an additional character that, so far, has been overlooked due to a focus on fixed specimens. To date, Fe–Br inclusions were only found in the genus *Robbea*, but they might not be restricted to only one genus within the Stilbonematinae and might also be found in other marine nematodes.

Our study highlights the value of voucher images of live organisms and the ability to link these with morphometry- and sequencing-based approaches. We highly recommend that the deposition of such voucher images in public data repositories should become the norm to enable their reanalysis at a later stage.

SUPPLEMENTARY DATA

Supplementary data are available at *Zoological Journal of the Linnean Society* online.

ACKNOWLEDGEMENTS

We thank the staff of the Carrie Bow Cay Marine Station, Belize, operated by the CCRE Program of the National Museum of Natural History (Washington, DC) for continued support over many years, the staff of

the Hydra Marine Station at Fetovaia (Elba, Italy) for their hospitality. We thank Prof. Ramon Rosello-Mora and his team from the l'Institut Mediterrani d'Estudis Avançats in Mallorca for their support in the sample collection. Collection of material in the Philippines was made possible by a gtz-grant to Bernardita Germano. We thank Brandon Seah and Yui Sato for material from Okinawa, Japan. Mag. Daniela Gruber from the Core Facility of Imaging (CIUS) at the University of Vienna was invaluable for the EDX study. We especially thank Prof. Dr Hans Leo Nemeschkal at the Department of Evolutionary Biology, Unit for Theoretical Biology, University of Vienna, who introduced us to multivariate analysis morphometry.

FUNDING

The study was supported by the Austrian Science Fund FWF grant Nr. P 31594-B29 (PI JAO) and the Max Planck Society via Nicole Dubilier (NL, HGV, BG). HGV was partially funded by the DFG (Heisenberggrant GR 5028/1-1). This is Contribution Number 1076 of the Carrie Bow Cay Marine Station.

CONFLICT OF INTEREST

The authors declare no conflict of interest.

DATA AVAILABILITY

All sequences generated for this study were deposited in GenBank. Alignments are deposited at figshare: 10.6084/m9.figshare.23303633.

REFERENCES

Ahmed M, Holovachov O. Description of a new marine predatory nematode *Latronema dyngi* sp. Nov. (Nematoda, Chromadorida, Selachinematidae) from the west coast of Sweden and an updated phylogeny of Chromadoria. *Marine Biodiversity* 2020;**50**:113. https://doi.org/10.1007/s12526-020-01129-w

Ahmed M, Boström S, Holovachov O. Revision of the genus *Cobbionema* Filipjev, 1922 (Nematoda, Chromadorida, Selachinematidae). *European Journal of Taxonomy* 2020;**702**. https://doi.org/10.5852/ejt.2020.702

Anisimova M, Gil M, Dufayard J-F *et al*. Survey of branch support methods demonstrates accuracy, power, and robustness of fast likelihood-based approximation schemes. *Systematic Biology* 2011;**60**:685–99. https://doi.org/10.1093/sysbio/syr041

Armenteros M, Rojas-Corzo A, Ruiz-Abierno A *et al*. Systematics and DNA barcoding of free-living marine nematodes with emphasis on tropical desmodorids using nuclear SSU rDNA and mitochondrial COI sequences. *Nematology* 2014a;**16**:979–89. https://doi.org/10.1163/15685411-00002824

Armenteros M, Ruiz-Abierno A, Decraemer W. Taxonomy of Stilbonematinae (Nematoda: Desmodoridae): description of two new and three known species and phylogenetic relationships within the family. *Zoological Journal of the Linnean Society* 2014b;**171**:1–21. https://doi.org/10.1111/zoj.12126

Bankevich A, Nurk S, Antipov D *et al*. SPAdes: a new genome assembly algorithm and its applications to single-cell sequencing. *Journal of Computational Biology* 2012;**19**:455–77. https://doi.org/10.1089/cmb.2012.0021

Bauer L. Molekulare Charakterisierung und Lokalisationsmuster zweier putativer Bakterien-permeabilisierender Proteine (BPI) eines marinen symbiotischen Nematoden. Master Thesis, University of Vienna, Austria, 2012. https://doi.org/10.25365/thesis.21863

Bauer-Nebelsick M, Blumer M, Urbancik W *et al*. The glandular sensory organ of Desmodoridae (Nematoda)—ultrastructure and phylogenetic implications. *Invertebrate Biology* 1995;**114**:211–9. https://doi.org/10.2307/3226876

Bickford D, Lohman DJ, Sodhi NS *et al*. Cryptic species as a window on diversity and conservation. *Trends in Ecology and Evolution* 2007;**22**:148–55. https://doi.org/10.1016/j.tree.2006.11.004

Bird A, McClure S, Nicholas W. Observations on crystalloid bodies in the pseudocoelom of *Eutobrilus heptapapillatus*. *Journal of Nematology* 1991;**23**:39.

Bonferroni C. Teoria statistica delle classi e calcolo delle probabilita. *Pubblicazioni Del R Istituto Superiore Di Scienze Economiche e Commericiali Di Firenze* 1936;**8**:3–62.

Boucher G. Nématodes des sables fins infralittoraux de la Pierre Noire (Manche occidentale). I. Desmodorida. *Bulletin Du Muséum National d'Histoire Naturelle* 1975;**325**:101–28.

Bulgheresi S, Schabussova I, Chen T *et al*. A new C-type lectin similar to the human immunoreceptor DC-SIGN mediates symbiont acquisition by a marine nematode. *Applied and Environmental Microbiology* 2006;**72**:2950–6. https://doi.org/10.1128/AEM.72.4.2950-2956.2006

Bulgheresi S, Gruber-Vodicka HR, Heindl NR *et al*. Sequence variability of the pattern recognition receptor Mermaid mediates specificity of marine nematode symbioses. *The ISME Journal* 2011;**5**:986–98. https://doi.org/10.1038/ismej.2010.198

Bushnell, B. (2014). *BBMap: A Fast, Accurate, Splice-Aware Aligner.* Berkeley, CA: Lawrence Berkeley National Lab.(LBNL).

Cipriani F, Felisaz F, Launer L *et al*. Automation of sample mounting for macromolecular crystallography. *Acta Crystallographica Section D: Biological Crystallography* 2006;**62**:1251–9. https://doi.org/10.1107/S0907444906030587

Cobb N. One hundred new nemas. *Contributions to a Science of Nematology* 1920;**9**:217–343.

Eickhoff MJ, Bassler BL. *Vibrio fischeri* siderophore production drives competitive exclusion during dual-species growth. *Molecular Microbiology* 2020;**114**:244–61. https://doi.org/10.1111/mmi.14509

Frenkiel L, Gros O, Mouëza M. Gill structure in *Lucina pectinata* (Bivalvia: Lucinidae) with reference to hemoglobin in bivalves with symbiotic sulphur-oxidizing bacteria. *Marine Biology* 1996;**125**:511–24. https://doi.org/10.1007/bf00353264

Gerlach S. Über einige Nematoden aus der Familie der Desmodoriden. *Zoologischer Anzeiger* 1950;**145**:178–98.

Gerlach SA. Die Nematodenbesiedlung des tropischen Brandungsstrandes von Pernambuco: Brasilianische Meeres-Nematoden, II. *Kieler Meeresforschungen* 1956;**12**:202–18.

Gerlach SA. *Robbea tenax* sp. N., ein merkwürdiger mariner Nematode von den Malediven. *Internationale Revue Der Gesamten Hydrobiologie Und Hydrographie* 1963;**48**:153–8. https://doi.org/10.1002/iroh.19630480106

Gribble GW. The diversity of naturally occurring organobromine compounds. *Chemical Society Reviews* 1999;**28**:335–46. https://doi.org/10.1039/A900201D

Gruber-Vodicka Harald R, Seah Brandon KB, Pruesse E. phyloFlash: rapid small-subunit rRNA profiling and targeted assembly from metagenomes. *MSystems* 2020;**5**:e00920–20. https://doi.org/10.1128/mSystems.00920-20

Guindon S, Dufayard J-F, Lefort V *et al*. New algorithms and methods to estimate maximum-likelihood phylogenies: assessing the performance of PhyML 3.0. *Systematic Biology* 2010;**59**:307–21. https://doi.org/10.1093/sysbio/syq010

Hopper BE, Cefalu RC. Free-living marine nematodes from Biscayne Bay, Florida V. Stilbonematinae: contributions to the taxonomy and morphology of the genus Eubostrichus Greeff and related genera. *Transactions of the American Microscopical Society* 1973;**92**:578–91. https://doi.org/10.2307/3225268

Inglis W. Interstitial nematodes from St. Vincent's Bay, New-Caledonia. *Expedition Francaise Sur Les Recifs Coralliens de La Nouvelle-Caledonie.* 1967;**2**:29–74.

Janssen HH, Oeschger R. The body wall of *Halicryptus spinulosus* (Priapulida)—Ultrastructure and changes induced by hydrogen sulfide. *Hydrobiologia* 1992;**230**:219–30. https://doi.org/10.1007/bf00036568

Kalyaanamoorthy S, Minh BQ, Wong TKF *et al*. ModelFinder: fast model selection for accurate phylogenetic estimates. *Nature Methods* 2017;**14**:587–9. https://doi.org/10.1038/nmeth.4285

Kampfer S, Sturmbauer C, Ott J. Phylogenetic analysis of rDNA sequences from adenophorean nematodes and implications for the Adenophorea–Secernentea controversy. *Invertebrate Biology* 1998;**117**:29–36. https://doi.org/10.2307/3226849

Kassambara A, Mundt F. Factoextra: extract and visualize the results of multivariate data analyses. *R Package Version 1.0.7*. 2020. https://CRAN.R-project.org/package=factoextra

Katoh K, Standley DM. MAFFT multiple sequence alignment software v.7: improvements in performance and usability. *Molecular Biology and Evolution* 2013;**30**:772–80. https://doi.org/10.1093/molbev/mst010

Katoh K, Toh H. Recent developments in the MAFFT multiple sequence alignment program. *Briefings in Bioinformatics* 2008;**9**:286–98. https://doi.org/10.1093/bib/bbn013

La Barre S, Potin P, Leblanc C *et al*. The halogenated metabolism of brown algae (Phaeophyta), its biological importance and its environmental significance. *Marine Drugs* 2010;**8**:988–1010. https://doi.org/10.3390/md8040988

Leisch N, Verheul J, Heindl NR *et al*. Growth in width and FtsZ ring longitudinal positioning in a gammaproteobacterial symbiont. *Current Biology: CB* 2012;**22**:R831–2. https://doi.org/10.1016/j.cub.2012.08.033

Leisch N, Pende N, Weber PM *et al*. Asynchronous division by non-ring FtsZ in the gammaproteobacterial symbiont of *Robbea hypermnestra*. *Nature Microbiology* 2016;**2**:16182. https://doi.org/10.1038/nmicrobiol.2016.182

Longford SR, Campbell AH, Nielsen S *et al*. Interactions within the microbiome alter microbial interactions with host chemical defences and affect disease in a marine holobiont. *Scientific Reports* 2019;**9**:1363. https://doi.org/10.1038/s41598-018-37062-z

Loy A, Schulz C, Lücker S *et al*. 16S rRNA gene-based oligonucleotide microarray for environmental monitoring of the Betaproteobacterial order 'Rhodocyclales'. *Applied and Environmental Microbiology* 2005;**71**:1373–86. https://doi.org/10.1128/AEM.71.3.1373-1386.2005

Mankowski A, Kleiner M, Erséus C *et al*. Highly variable fidelity drives symbiont community composition in an obligate symbiosis. *BioRxiv* 2021. https://doi.org/10.1101/2021.04.28.441735

McDonald KL. Rapid embedding methods into epoxy and LR white resins for morphological and immunological analysis of cryofixed biological specimens. *Microscopy and Microanalysis* 2014;**20**:152–63. https://doi.org/10.1017/S1431927613013846.

van Megen H, van den Elsen S, Holterman M *et al*. A phylogenetic tree of nematodes based on about 1200 full-length small subunit ribosomal DNA sequences. *Nematology* 2009;**11**:927–50. https://doi.org/10.1163/156854109x456862

Millward RN. Intracellular inclusions in the nematode *Tripyloides marinus* from metal-enriched and cleaner estuaries in Cornwall, south-west England. *Journal of the Marine Biological Association of the United Kingdom* 1996;**76**:885–95. https://doi.org/10.1017/s0025315400040868.

Minh BQ, Nguyen MAT, von Haeseler A. Ultrafast approximation for phylogenetic bootstrap. *Molecular Biology and Evolution* 2013;**30**:1188–95. https://doi.org/10.1093/molbev/mst024

Moens T, Braeckman U, Derycke S *et al*. 3. Ecology of free-living marine nematodes. In: Schmidt-Rhaesa A (ed.), *Nematoda*. Berlin, Boston: De Gruyter, 2013, 109–52. https://doi.org/10.1515/9783110274257.109

Montanaro J, Gruber D, Leisch N. Improved ultrastructure of marine invertebrates using non-toxic buffers. *PeerJ* 2016;**4**:e1860–e1860. https://doi.org/10.7717/peerj.1860

Morris AW, Riley JP. The bromide/chlorinity and sulphate/chlorinity ratio in sea water. *Deep Sea Research and Oceanographic Abstracts* 1966;**13**:699–705. https://doi.org/10.1016/0011-7471(66)90601-2.

Nebelsick M, Blumer M, Novak R *et al*. A new glandular sensory organ in *Catanema* sp. (Nematoda, Stilbonematinae). *Zoomorphology* 1992;**112**:17–26. https://doi.org/10.1007/bf01632991

Nguyen L-T, Schmidt HA, von Haeseler A *et al*. IQ-TREE: a fast and effective stochastic algorithm for estimating maximum-likelihood phylogenies. *Molecular Biology and Evolution* 2015;**32**:268–74. https://doi.org/10.1093/molbev/msu300

Nicholas WL, Goodchild DJ, Stewart A. The mineral composition of intracellular inclusions in nematodes from thiobiotic mangrove mud-flats. *Nematologica* 1987;**33**:167–79. https://doi.org/10.1163/187529287x00308.

Ott J. New freeliving marine nematodes from the West Atlantic. I. Four new species from Bermuda with a discussion of the genera Cytolaimium and Rhabdocoma Cobb, 1920. *Zoologischer Anzeiger* 1977;**198**:120–38.

Ott J, Novak R. Living at an interface: meiofauna at the oxygen/sulfide boundary of marine sediments. In: Tyler PA (ed.), *In Reproduction, Genetics and Distribution of Marine Organisms*. Fredenborg: Olsen & Olsen, 1989, 415–22.

Ott JA, Novak R, Schiemer F *et al*. Tackling the sulfide gradient: a novel strategy involving marine nematodes and chemoautotrophic ectosymbionts. *Marine Ecology* 1991;**12**:261–79. https://doi.org/10.1111/j.1439-0485.1991.tb00258.x

Ott J, Bauer-Nebelsick M, Novotny V. The genus Laxus Cobb, 1984 (Stilbonematinae: Nematoda): description of two new species with ectosymbiotic chemoautotrophic bacteria. *Proceedings of the Biological Society of Washington* 1995;**108**:508–27.

Ott J, Bright M, Bulgheresi S. Symbioses between marine nematodes and sulfur-oxidizing chemoautotrophic bacteria. *Symbiosis* 2004;**36**:103–26.

Ott JA, Gruber-Vodicka HR, Leisch N *et al*. Phylogenetic confirmation of the genus Robbea (Nematoda: Desmodoridae, Stilbonematinae) with the description of three new species. *Systematics and Biodiversity* 2014;**12**:434–55. https://doi.org/10.1080/14772000.2014.941038

Ott J, Pröts P, Scharhauser F. A new marine nematode, *Catanema schiemeri* sp. nov. (Desmodoroidea) with multiple prokaryotic symbionts. *Acta ZooBot Austria* 2020;**157**:275–87.

Park JS, Ryu E-J, Li L *et al*. New bicyclic brominated furanones as potent autoinducer-2 quorum-sensing inhibitors against bacterial biofilm formation. *European Journal of Medicinal Chemistry* 2017;**137**:76–87. https://doi.org/10.1016/j.ejmech.2017.05.037

Parrow NL, Fleming RE, Minnick MF. Sequestration and scavenging of iron in infection. *Infection and Immunity* 2013;**81**:3503–14. https://doi.org/10.1128/IAI.00602-13

Paul NA, de Nys R, Steinberg PD. Seaweed–herbivore interactions at a small scale: direct tests of feeding deterrence by filamentous algae. *Marine Ecology Progress Series* 2006;**323**:1–9. https://doi.org/10.3354/meps323001

Pende N, Leisch N, Gruber-Vodicka HR *et al*. Size-independent symmetric division in extraordinarily long cells. *Nature Communications* 2014;**5**:4803. https://doi.org/10.1038/ncomms5803

Pende N, Wang J, Weber PM *et al*. Host-polarized cell growth in animal symbionts. *Current Biology: CB* 2018;**28**:1039–1051.e5. https://doi.org/10.1016/j.cub.2018.02.028

Pereira TJ, De Santiago A, Schuelke T *et al*. The impact of intragenomic rRNA variation on metabarcoding-derived diversity estimates: a case study from marine nematodes. *Environmental DNA* 2020;**2**:e77. https://doi.org/10.1002/edn3.77

Platt HM, Zhang ZN. New species of marine nematodes from Loch Ewe, Scotland. *Bulletin of the British Museum (Natural History) Zoology* 1982;**42**:227–46.

Plessner O, Klapatch T, Guerinot ML. Siderophore utilization by *Bradyrhizobium japonicum*. *Applied and Environmental Microbiology* 1993;**59**:1688–90. https://doi.org/10.1128/aem.59.5.1688-1690.1993

Polikarpov M, Bourenkov G, Snigireva I *et al*. Visualization of protein crystals by high-energy phase-contrast X-ray imaging. *Acta Crystallographica Section D: Structural Biology* 2019;**75**:947–58. https://doi.org/10.1107/S2059798319011379

Polz MF, Distel DL, Zarda B *et al*. Phylogenetic analysis of a highly specific association between ectosymbiotic, sulfur-oxidizing bacteria and a marine nematode. *Applied and Environmental Microbiology* 1994;**60**:4461–7. https://doi.org/10.1128/aem.60.12.4461-4467.1994

R Team DC. *A Language and Environment for Statistical Computing*. 2009. Http://Www.R-Project.Org(3 July 2023, date last accessed).

Sankari S, Babu VMP, Bian K *et al*. A haem-sequestering plant peptide promotes iron uptake in symbiotic bacteria. *Nature Microbiology* 2022;**7**:1453–65. https://doi.org/10.1038/s41564-022-01192-y

Scharhauser F, Zimmermann J, Ott JA *et al*. Morphology of obligate ectosymbionts reveals *Paralaxus* gen. nov.: a new circumtropical genus of marine stilbonematine nematodes. *Zoologica Scripta* 2020;**49**:379–94. https://doi.org/10.1111/zsc.12399

Schindelin J, Arganda-Carreras I, Frise E *et al.* Fiji: an open-source platform for biological-image analysis. *Nature Methods* 2012;**9**:676–82. https://doi.org/10.1038/nmeth.2019

Schleicher TR, Nyholm SV. Characterizing the host and symbiont proteomes in the association between the bobtail squid, *Euprymna scolopes*, and the bacterium, *Vibrio fischeri*. *PLoS One* 2011;**6**:e25649. https://doi.org/10.1371/journal.pone.0025649

Stevenson BM, Howard F. Properties of sufficiency and statistical tests. *Proceedings of the Royal Society of London. Series A-Mathematical and Physical Sciences* 1937;**160**:268–82. https://doi.org/10.1098/rspa.1937.0109

Suzuki R, Terada Y, Shimodaira H. *Pvclust: Hierarchical Clustering with P-Values via Multiscale Bootstrap Resampling. R package, v. 2.2–0.* 2019. https://CRAN.R-project.org/package=pvclust (2 May 2023, date last accessed).

Tchesunov AV. Marine free-living nematodes of the subfamily Stilbonematinae (Nematoda, Desmodoridae): taxonomic review with descriptions of a few species from the Nha Trang Bay, Central Vietnam. *Meiofauna Marina* 2013;**20**:71–94.

Thiermann F, Windoffer R, Giere O. Selected meiofauna around shallow water hydrothermal vents off Milos (Greece): ecological and ultrastructural aspects. *Vie et Milieu/Life and Environment* 1994;**44**:215–26.

Tukey JW. Comparing individual means in the analysis of variance. *Biometrics* 1949;**5**:99–114. https://doi.org/10.2307/3001913

Urbancik W, Bauer-Nebelsick M, Ott JA. The ultrastructure of the cuticle of Nematoda I. The body cuticle within the Stilbonematinae (Adenophorea, Desmodoridae). *Zoomorphology* 1996a;**116**:51–64. https://doi.org/10.1007/bf02526870

Urbancik W, Novotny V, Ott JA. The ultrastructure of the cuticle of Nematoda. II. The cephalic cuticle of Stilbonematinae (Adenophorea, Desmodoridae). *Zoomorphology* 1996b;**116**:65–75. https://doi.org/10.1007/bf02526871

Vitiello P. New species of Desmodorida (Nematoda) from the Provence coast. *Tethys* 1973;**5**:137–46.

Weber PM, Moessel F, Paredes GF *et al*. A bidimensional segregation mode maintains symbiont chromosome orientation toward its host. *Current Biology: CB* 2019;**29**:3018–3028.e4. https://doi.org/10.1016/j.cub.2019.07.064

Weber PM, Paredes GF, Viehboeck T *et al*. FtsZ-mediated fission of a cuboid bacterial symbiont. *IScience* 2022;**25**:103552. https://doi.org/10.1016/j.isci.2021.103552

Weisburg WG, Barns SM, Pelletier DA *et al*. 16S ribosomal DNA amplification for phylogenetic study. *Journal of Bacteriology* 1991;**173**:697–703. https://doi.org/10.1128/jb.173.2.697-703.1991

Whitley E, Ball J. Statistics review 5: comparison of means. *Critical Care (London, England)* 2002;**6**:424–8. https://doi.org/10.1186/cc1548

Wick RR, Schultz MB, Zobel J *et al*. Bandage: interactive visualization of de novo genome assemblies. *Bioinformatics* 2015;**31**:3350–2. https://doi.org/10.1093/bioinformatics/btv383

Windoffer AJ, Frank M, Jens K *et al*. Sulphide-induced metal precipitation in the mantle edge of *Macoma balthica* (Bivalvia, Tellinidae)—a means of detoxification. *Marine Ecology Progress Series* 1999;**187**:159–70.

Wohlgemuth SE, Arp AJ, Bergquist D *et al*. Rapid induction and disappearance of electron-dense organelles following sulfide exposure in the marine annelid *Branchioasychis americana*. *Invertebrate Biology* 2007;**126**:163–72. https://doi.org/10.1111/j.1744-7410.2007.00086.x

Zang T, Lee BWK, Cannon LM *et al*. A naturally occurring brominated furanone covalently modifies and inactivates LuxS. *Bioorganic and Medicinal Chemistry Letters* 2009;**19**:6200–4. https://doi.org/10.1016/j.bmcl.2009.08.095

Zimmermann J, Wentrup C, Sadowski M *et al*. Closely coupled evolutionary history of ecto- and endosymbionts from two distantly related animal phyla. *Molecular Ecology* 2016;**25**:3203–23. https://doi.org/10.1111/mec.13554